AEROSPACE INFORMATION REPORT

AIR1419™ REV. D

Issued 1983-05
Reaffirmed 2011-07
Revised 2023-08

Superseding AIR1419C

Inlet Total-Pressure Distortion Considerations for Gas-Turbine Engines

RATIONALE

The intent of this document is to provide a basic understanding of the effects of inlet total-pressure distortion on the performance of gas turbine engines, particularly in military applications.

In Revision D, only changes to Section 3 have been made to make the document consistent with ARP1420C and ARP6420. These changes include removing definitions inconsistent with the intent of the previously mentioned SAE Aerospace Recommended Practices (ARPs) and to add clarity to the remaining definitions.

In Revision C, an introduction was incorporated to include material inadvertently omitted from Revision B. The introduction describes usages of distortion assessments during typical phases of aircraft propulsion system development and operation.

Revisions to AIR1419B were made to reflect new knowledge in the following areas:

- Computational fluid dynamics (CFD) has become widely used for design and analysis,
- Highly offset inlets have imposed additional challenges,
- Full authority digital electronic control (FADEC) systems have become commonplace,
- New methods of distortion synthesis have been developed,
- New instrumentation techniques have been developed,
- New techniques for data acquisition, storage, and processing have been developed,
- Testing methodology/procedures have changed, and
- Some previously state-of-the-art techniques have become obsolete.

The philosophy that was adopted to implement the changes was:

- Only material was added that did not exist in original document, and
- Dated references to “state-of-the-art,” “current technology,” etc. were revised.

SAE Executive Standards Committee Rules provide that: “This report is published by SAE to advance the state of technical and engineering sciences. The use of this report is entirely voluntary, and its applicability and suitability for any particular use, including any patent infringement arising therefrom, is the sole responsibility of the user.”

SAE reviews each technical report at least every five years at which time it may be revised, reaffirmed, stabilized, or cancelled. SAE invites your written comments and suggestions.

Copyright © 2023 SAE International

All rights reserved. No part of this publication may be reproduced, stored in a retrieval system or transmitted, in any form or by any means, electronic, mechanical, photocopying, recording, or otherwise, without the prior written permission of SAE.

TO PLACE A DOCUMENT ORDER: **Tel: 877-606-7323 (inside USA and Canada)**
Tel: +1 724-776-4970 (outside USA)
Fax: 724-776-0790
Email: CustomerService@sae.org
SAE WEB ADDRESS: **http://www.sae.org**

For more information on this standard, visit
https://www.sae.org/standards/content/AIR1419D/

Documents
Document Sharing Hub

Full document details: SAE AIR1419D

PREFACE

Industry and government agencies concerned with aircraft design and operation recognize a need to improve methodology and communication on spatial total-pressure distortion aspects of the inlet/engine compatibility problem. The appearance of modern turbofan engines in the late 1960s focused attention on this need, and there followed a period of intense activity to develop engineering techniques for assuring adequate stability. These techniques were identified, formulated, and exercised independently in various parts of industry to solve flow distortion problems on specific systems. The aircraft and engine companies form a matrix of cooperative engineering activity in the international military and civil aircraft market, and a third dimension is added by the group of customers. The three groups needed to consolidate individual experience, establish common ground, and gain a perspective concerning the applicability and accuracy of these techniques. Adequate resolution of the aircraft/engine stability problem would depend upon generating generally usable guidelines addressing analysis, test, data processing, and information transfer which would be applied in a manner consistent with the expected severity of the problem.

The SAE International Aerospace Council Divisional Technical Committee S-16 (Turbine Engine Inlet Flow Distortion Committee) was formed in 1972 to examine the aircraft gas turbine engine/inlet compatibility development process, as affected by flow distortion, to assess what experience was common throughout industry, or what could be agreed as desirable to make common. The Committee formulated a number of guidelines to improve communications and minimize repetitive workloads among program participants. It recognized that practices employed to cope with flow distortion effects were young and changing and that in several critical areas, practice was not sufficiently common or defined to warrant establishing guidelines. For these reasons, the guidelines were purposely limited, and were organized and published in March 1978 as Aerospace Recommended Practice ARP1420, Gas Turbine Engine Inlet Flow Distortion Guidelines. ARP1420 was circulated widely in the U.S. and European aeronautical industries. Significant comments and opinions were expressed, and were carefully considered by the Committee prior to submitting the ARP to the SAE Aerospace Council for publication.

The S-16, in its proceedings, produced a wealth of information which, in its entirety, contained a significant part of the flow-distortion-related corporate knowledge of the industry as it existed in the mid-1970s time period. The Committee decided that this information, organized into a generally available document, would provide a source of knowledge for engineers new to the problems of inlet-engine compatibility. The Committee, therefore, compiled Aerospace Information Report AIR1419, Inlet-Total-Pressure Distortion Considerations for Gas-Turbine Engines, to amplify the information contained in ARP1420 and to provide a corporate memory.

SAE Technical Committee S-16, through its members and liaison representatives, represents a cross section of the part of government and industry having the major share of the responsibility for assuring economical, safe, and instability-free propulsion systems. The organizations that sponsor S-16 and make possible, through the members and representatives, ARP1420, AIR1419, and other inlet distortion documents, should be commended. These documents exist today because of their active concern for the distortion problem and their willingness to provide resources to obtain solutions. The members and representatives collectively contributed hundreds of hours of work between Committee meetings to assure worthwhile results and productive meetings.

INTRODUCTION

This document contains engineering information for use as reference material and for guidance. Inlet total-pressure distortion and other forms of flow distortion that can influence inlet/engine compatibility require examination to establish the effect on engine stability and performance. This report centers on inlet-generated total-pressure distortion measured at the Aerodynamic Interface Plane (AIP), not because this is necessarily the sole concern, but because it has been given sufficient attention in the aircraft and engine communities to produce generally accepted engineering practices for dealing with it. The report does not address procedures for dealing with performance destabilizing influences other than those due to total-pressure distortion, or with the effects of any distortion on aeroelastic stability. The propulsion system designer must be careful to assure that, throughout the development process, other forms of inlet flow distortion, which can have just as serious effects on system stability and performance, have been effectively addressed.

The report deals with spatial total-pressure distortion, as defined by an array of high-response total-pressure probes. Time-variant total-pressure distortion, synthesized from statistical data, can provide useful information. However, the consensus of SAE S-16 is that such techniques are not developed sufficiently to permit general guidelines to be formulated.

Documents
Document Sharing Hub
Full document details: SAE AIR1419D

Concepts which are fundamental to this report are:

a. Inlet flow quality can be characterized, in a form relevant to engine distortion response, with numerical descriptors derived from an array of high-response total-pressure probes.

b. Propulsion system stability can be controlled by the aircraft and engine designers.

c. Engine stability can be demonstrated by tests using equivalent levels of steady state distortion.

The report is organized into nine technical sections (Sections 3 through 11) followed by a summary, expanding upon the ideas and recommended practice set forth in ARP1420. Sections 3 and 4 deal with stability margin, loss of stability pressure ratio, and procedures for correlating the loss of stability pressure ratio with total-pressure distortion. Through use of the terms and procedures discussed earlier, Sections 5 and 6 develop engine stability and performance assessment techniques for handling total-pressure distortion by putting them into context with other destabilizing influences and performance detriments. Section 7 describes various test procedures, equipment, and methods currently available for generating the information needed to apply distortion assessment techniques. Section 8 discusses interface instrumentation, data-acquisition system accuracy, frequency response, record length, recording systems, and the data management procedures necessary to minimize communication errors among participating organizations. Section 9 reviews available computational techniques that can be used to model compressor response to inlet distortion. Section 10 provides a brief discussion of other forms of distortion at the inlet/engine Aerodynamic Interface Plane, while Section 11 describes other factors that can affect engine operability, along with a review of other considerations involved in assessments of inlet/engine compatibility. A summary of the information in the document is presented in Section 12.

The distortion descriptor is the vehicle by which engine reaction to inlet distortion is forecast and assessed, from program outset well into field use of the system. ARP1420 defines the distortion descriptor as a non-dimensional, numerical representation of the measured inlet pressure distribution, and provides a means for identifying critical inlet flow distortions and for communicating during propulsion system development. Central issues are the distortion descriptors, methods of correlating them with performance and stability changes, and test and information acquisition techniques. Use and accuracy of the descriptors vary, depending upon the stage of the engine development, but their definitions and purpose remain constant: to assess status, forecast stability, and identify required engineering activity.

The activities associated with distortion descriptor use can be categorized for convenience in phases (Table 1), recognizing that there is little consensus concerning the definitions of these phases and that no clear lines of demarcation exist between them.

Documents
Document Sharing Hub
Full document details: SAE AIR1419D

Table 1 - Distortion assessment uses during the propulsion system life cycle

PHASE	ACTIVITY	AIRFRAME MANUFACTURER	ENGINE MANUFACTURER	STATUS AT END OF PHASE
1. Conceptual Studies	1. Analytical evaluation of candidate aircraft and propulsion system configurations 2. Mission evaluation	1. Establish inlet distortion trends 2. Evaluate alternative inlet designs and locations 3. Estimate maneuver limitations 4. Evaluate armament locations 5. Evaluate airframe/propulsion system integration	1. Include inlet distortion effects in selection of engine configurations based on past experience	1. Candidates that can potentially meet requirements 2. Preliminary definition of stability requirements
2. Preliminary Design	1. Design, analysis, and test of inlet and engine components 2. System design selection 3. Establish flight maneuver envelope goals	1. Determine preliminary distortion characteristics 2. Evaluate airframe/propulsion system integration 3. Determine preliminary airflow matching 4. Establish distortion level goals for inlet 5. Perform periodic stability assessments jointly with engine manufacturer	1. Define stability margin requirements and select compression system design 2. Define engine distortion tolerance goals	1. Distortion goals defined 2. Mission defined 3. Inlet/engine compatibility approach defined 4. Propulsion system defined
3. Development	1. Development of required quality through continuing analysis and test of airframe and engine components and systems	1. Verify airflow matching 2. Define inlet design effects on distortion 3. Identify critical distortion patterns/levels 4. Establish distortion level commitments 5. Perform periodic stability assessment jointly with engine manufacturer	1. Establish distortion level commitments 2. Define patterns for qualification tests 3. Correlate stability margin and performance changes due to distortion	1. Distortion commitments agreed upon 2. Data bank established 3. Full scale inlet/engine compatibility tests performed if necessary 4. Propulsion system ready for production
4. Engine Qualification or Certification	1. Demonstration of required levels of propulsion system stability/compatibility	1. Perform joint stability assessments 2. Perform wind tunnel tests of production changes 3. Perform installed performance calculations of “status” configuration	1. Demonstrate engine operation with distortion	1. Propulsion system with acceptable performance and stability at specified conditions
5. Flight Test	1. Demonstration of propulsion system operation 2. Inlet and engine improvements flight-tested to produce best combination of performance and stability	1. Establish flight/maneuver envelopes 2. Determine distortion levels at propulsion system limits 3. Resolve deficiencies 4. Compare flight test and wind tunnel data	1. Correlate flight and development data 2. Identify sources of flight-revealed stability problems	1. Propulsion system performance and stability demonstrated over flight and maneuver envelopes
6. Operational	1. Collection of operational data 2. Propulsion system modified as necessary	1. Evaluate propulsion system modifications 2. Evaluate operational anomalies	1. Service, overhaul, and modification evaluation 2. Operational troubleshooting	1. Operational capability monitored

AVA Documents Document Sharing Hub

Full document details: SAE AIR1419D

1. Conceptual Studies Phase

This phase, the initial step in the life cycle for an aircraft system, is characterized by analytical evaluations of candidate aircraft/propulsion system configurations. Generally, no new testing is planned for this phase and information for the evaluations is based on historical sources. Recognition of and planning for a stability assessment during concept evaluation serves to assure that (1) distortion effects are a prime consideration in the selection of the candidate propulsion system, (2) those conditions that are considered areas of risk are given particular attention during the subsequent design and development phases, and (3) distortion patterns, inherent to the type of aircraft inlet, are defined to enable the engine to be designed with consideration for predominant patterns.

The distortion descriptor is used to determine the relative standing of several candidate inlet configurations. Specific items to be evaluated include design concept and location, inlet performance, and aircraft maneuverability, as affected by distortion, armament location, approximate inlet/engine matching characteristics, overall distortion trends with inlet geometry, and primary and secondary airflow requirements. The descriptor is used to evaluate the stability characteristics of candidate compressor and engine configurations, their sensitivity to distortion, the stability margin available for distortion, and potential problems peculiar to the various thermodynamic cycles and engine control modes.

This phase should end when the overall aircraft and the propulsion system configurations that can best meet generalized mission requirements are defined. Limiting operating conditions within the anticipated flight envelope should have been identified, including but not limited to those due to inlet total-pressure distortion, unstart, buzz, temperature distortion, swirl, water ingestion, armament-exhaust-gas ingestion, and unusual amounts of engine bleed or power extraction. The consequence of loss of stability margin associated with these conditions should have been assessed and a procedure established for continuously tracking compatibility throughout the development program.

2. Preliminary Design Phase

This phase is the second step in the development cycle, during which mission requirements are defined in more detail and a baseline vehicle has been selected. Airframe-inlet integration and inlet component testing have begun with small scale models to update compatibility estimates and to define the extent of required development work. Preliminary indications of the extent of the distortion problems to be expected are identified using data obtained from steady state and dynamic probes located at the inlet/engine aerodynamic interface plane. Fan and compressor performance maps, flow path geometry, and blade sizes are estimated. Where appropriate, applicable engine components are tested with distortion patterns characteristic of the inlets being considered by the airframe contractor.

The distortion descriptor is used to aid in selecting those inlet/airframe components that result in a favorable flow field. Preliminary distortion characteristics are determined for critical aircraft operating conditions. The distortion descriptors are used to assess the effects of distortion on the engine and its components. Engine simulations, with transient capability and control logic, are initiated and used to perform preliminary engine stability audits, to define engine stability margin utilization, and to aid in establishing distortion goals for the inlet.

Engine distortion tolerance estimates are used to establish the allowable airflow range for inlet/engine matching, supercritical or subcritical limits, start/unstart procedures, control criteria, bleed configuration, boundary layer diverter design, noise requirements, maneuver capability, lip shape and radius, low-speed flow augmentation, and low-speed crosswind capability.

At the end of this phase, initial stability audit coordination has occurred between engine and airframe companies. The basic inlet and engine configurations have been defined but require further refinement. The vehicle mission has become well-defined. Provisions for coordinating any mission changes will have been made. Agreement should exist between airframe and engine contractors on:

- The distortion goals for the inlet and the engine at specific points within the flight envelope. These represent the maximum level of distortion the inlet will generate and the level the engine will tolerate.

- The type, severity, and number of equivalent classical patterns to be used during initial development testing.

Documents
Document Sharing Hub
Full document details: SAE AIR1419D

- The distortion patterns from subscale inlet testing to be used for engine development tests.

- A well-defined compatibility program including the definition of the data transmission formats, test sequence, criteria for decision making, the scope of dynamic distortion tests, demonstration points, type of instrumentation, and location of aerodynamic interface plane.

3. Development Phase

This phase starts when system mechanical configurations are defined and terminates when the propulsion system is ready for field use. The airframe, inlet, and engine configurations are refined through extensive test programs. The performance and compatibility of the airframe/inlet system are developed through wind-tunnel tests of large-scale models, and of the engine, through engine and component tests using suitable distortion generators. A full complement of dynamic instrumentation, located at the agreed AIP, is utilized during testing. Prior inlet distortion and engine tolerance commitments are updated based on realistic test data and changing requirements.

Updated stability margin and stability pressure ratio changes due to distortion are obtained from compressor rig and engine tests with inlet distortion. Distortion stability coefficients are adjusted correspondingly, and the process is repeated as engine design changes occur. The descriptor is used to verify inlet distortion levels, and design variables such as throat height, ramp position, cowl shape, bleed and bypass are examined for their effects on distortion. Updated distortion patterns, obtained from wind tunnel and flight tests, are used to refine stability and performance assessments. Descriptors and engine simulations are used to focus attention on components requiring further development. At the end of this phase, the airframe and engine have demonstrated compatibility throughout the required flight envelope.

4. Engine Qualification or Certification Phase

This phase represents the period during which tests are performed to clear the engine for initial flight testing, for limited production, and eventually, for full production. Qualification or certification requires quantitative assessments of engine performance and stability at a number of selected conditions. Distortion patterns are used during this phase to define the inlet/engine interface test conditions. The test conditions are defined in terms that include:

- Inlet/engine interface conditions
    - Airflow
    - Total pressure (local point-by-point values)
    - Total temperature
    - Altitude ambient pressure
- Installation interface conditions (aircraft service requirements)
    - Customer bleed
    - Power extraction
- Engine operating conditions
    - Engine power setting
    - Engine service bleeds (inter-compressor, anti-ice)
    - Control trim status

At the conclusion of this phase, the engine configuration will have demonstrated acceptable performance and stability for the specified sets of operating conditions.

Documents
Document Sharing Hub
Full document details: SAE AIR1419D

5. Flight Test Phase

Distortion testing through the early part of the development phase defines necessary design changes and provides an assessment of system performance and stability well in advance of flight. Flight testing may identify design changes and may uncover problems requiring further development because ground test facilities are limited in their ability to simulate the full flight and maneuver envelopes.

The primary engine uses of distortion descriptors are to correlate flight and ground test data, and to identify sources of flight-revealed performance and stability problems. Comparisons are made with previous engine stability predictions at specific steady-state and transient operating conditions. Stability assessment procedures may be updated and improved. Flight stability limits are identified and tracked in terms of descriptor level, aircraft Mach number, altitude, attitude, and inlet and engine control parameters.

The flight test phase is complete when adequate aircraft propulsion system performance and stability have been demonstrated over the flight and maneuver envelopes and there are no further requirements for flight-generated compatibility information prior to certification for full production.

6. Operational Phase

During this phase, system engineering changes, alterations in aircraft usage, maintenance effects, and aging effects are assessed for their impact upon inlet/engine compatibility. If additional testing and instrumentation are required, use of the distortion descriptors would be identical to that previously described in the flight test phase.

The complexity and expense of a compatibility program to execute the multi-phased process described will depend on system requirements. The program for a re-engining of an existing aircraft, or development of a podded installation for which significant background data exist based on similar designs and similar applications, may be uncomplicated and inexpensive to execute. More stringent mission requirements may force severe departures from experience, thus incurring added risk and therefore added program complexity and expense. The information in this report can be used as necessary to create a development method to minimize the risk of inlet/engine compatibility problems. The degree to which information regarding descriptor formulation and use, assessment techniques, and testing outlined in this document is applied to a specific program should be consistent with the expected severity of the compatibility problem.

TABLE OF CONTENTS

1. SCOPE 14
1.1 Purpose 14

2. REFERENCES 14
2.1 Applicable Documents 14
2.1.1 SAE Publications 14
2.2 Applicable References 15
2.3 Related Publications 19
2.4 Symbols and Abbreviations 20

3. STABILITY MARGIN AND LOSS OF STABILITY PRESSURE RATIO 27
3.1 ARP1420 Definitions and Rationale 27
3.2 Recommended Definitions of Stability Margin 31
3.3 Stability Margin with Inlet Distortion 31
3.4 Stability Limit Line Extrapolation in the Compressor Overspeed Region 32

4. STABILITY PRESSURE RATIO CORRELATION 34
4.1 Distortion Descriptor Element Definitions 34
4.1.1 Circumferential Distortion Elements - One-Per-Rev Patterns 35
4.1.2 Circumferential Distortion Elements - Multiple-Per-Rev Patterns 36
4.1.3 Radial Distortion Elements 37
4.2 Rationale for Element Definitions 38
4.3 Sample Element Calculations 38
4.4 Example Distortion Patterns 43
4.4.1 180 Degrees One-Per-Rev Circumferential Distortion Pattern 43

Document Sharing Hub

Full document details: SAE AIR1419D

4.4.2 Hub-Radial Distortion Pattern 44
4.4.3 Tip-Radial Distortion Pattern 45
4.4.4 180 Degrees One-Per-Rev + Hub-Radial Combined Distortion Pattern 46
4.4.5 180 Degrees One-Per-Rev + Tip-Radial Combined Distortion Pattern 47
4.4.6 90 Degrees One-Per-Rev + Tip-Radial Combined Distortion Pattern 48
4.4.7 Two-Per-Rev with Lows Closer than 25 Degrees and with Tip-Radial Distortion Pattern 49
4.4.8 Two-Per-Rev with Lows Further Apart than 25 Degrees and with Tip-Radial Distortion Pattern 50
4.4.9 Aircraft Pattern 51
4.5 Correlation Methods 52
4.5.1 Method A 53
4.5.2 Method B 61
4.5.3 Method C 73
4.5.4 Substantiation of Correlation Methods 78
4.6 Inlet Data Screening 78
4.6.1 General Considerations 78
4.6.2 Examples of Engine Dependency 83
4.6.3 Inlet Data Screening Techniques 83
4.6.4 Inlet Data Filtering (Averaging) 84
4.7 Independent Control of Variable Geometry 85

5. STABILITY ASSESSMENT 85
5.1 Stability Assessment Philosophy 86
5.2 Stability Assessment Procedure 89
5.3 Distortion Stability Assessment 93
5.3.1 Circumferential Distortion 94
5.3.2 Radial Distortion 99
5.3.3 Combined Circumferential and Radial Distortion 102

6. PERFORMANCE ASSESSMENT 105
6.1 Inlet Pressure Recovery and Distortion 105
6.1.1 Inlet Type/Location - Distortion Characteristics 105
6.1.2 Face-Average Total Pressure 108
6.1.3 Inlet Data Acquisition 109
6.2 Engine Performance Data 109
6.2.1 Compression Components Response to Distortion - Examples 110
6.2.2 Engine Response to Distortion - Examples 116
6.3 Assessment Procedures 123
6.3.1 Performance Synthesis 124
6.3.2 Performance Testing 129
6.4 Time-Variant Distortion 130

7. DISTORTION TESTING 130
7.1 Inlet and Aircraft Component Tests 131
7.1.1 Inlet Development Tests 132
7.1.2 Inlet Verification Tests 136
7.2 Engine and Engine Component Tests 137
7.2.1 Uniform Steady-State Inlet Flow 139
7.2.2 Steady-State Total-Pressure Distortion 142
7.2.3 Time-Variant Total-Pressure Distortion 146
7.3 Propulsion System Tests 150
7.3.1 Static Tests 151
7.3.2 Wind Tunnel Tests 152
7.3.3 Flight Tests 154
7.4 Stability Assessment Verification 155
7.5 Performance Assessment Verification 160

Documents
Document Sharing Hub
Full document details: SAE AIR1419D

8. INTERFACE INSTRUMENTATION AND DATA MANAGEMENT 163
8.1 Applications 170
8.2 Transducer/Probe Characteristics 173
8.2.1 Frequency Response 174
8.2.2 Probe Size Criteria 174
8.3 Data Acquisition System 176
8.3.1 General Description 176
8.3.2 System Accuracy 176
8.3.3 Frequency Response 181
8.3.4 Record Length 182
8.3.5 Recording Systems 182
8.4 Data Editing 183
8.4.1 Data and Time Segment Identification 184
8.4.2 Identification of Erroneous Signals 184
8.4.3 Probe Substitution Techniques 186
8.5 Data Reduction 189
8.5.1 Conversion to Engineering Units 189
8.5.2 Filtering 190
8.5.3 Frequency Analyses 192
8.6 Data Formats 198
8.6.1 Data Transmission 198
8.6.2 Time Histories 198
8.6.3 Distortion Patterns 200
8.6.4 Data Archival 202

9. COMPUTATIONAL TECHNIQUES TO EVALUATE COMPRESSION SYSTEM RESPONSE TO INLET DISTORTION 202
9.1 Meanline and Streamline Curvature Performance Simulations 203
9.2 One-Dimensional Dynamic Models 205
9.3 Parallel Compressor Models 207
9.4 Two-Dimensional Axial-Circumferential Models 209
9.5 Three-Dimensional Euler Models 209
9.6 Three-Dimensional Navier-Stokes Models 210

10. OTHER FORMS OF DISTORTION 211
10.1 Total-Temperature Distortion 211
10.2 Planar Waves 213
10.3 Swirl (Flow Angularity) Distortion 214
10.4 Distortion and Loss of Stability Pressure Ratio Estimation Techniques 215
10.5 Statistical Stability Assessment 216

11. OTHER OPERABILITY ISSUES 216
11.1 Aeromechanical Aspects 216
11.2 Compressor Post-Stall Behavior 218
11.3 Rig-to-Engine Differences 220
11.4 Water Ingestion 220
11.5 Inclement Weather 220
11.6 Catapult Steam Ingestion 222
11.7 Effects of Distortion on Engine Components Downstream of the Compression System 223

12. SUMMARY 223

13. NOTES 224
13.1 Revision Indicator 224

Documents
Document Sharing Hub
Full document details: SAE AIR1419D

Figure 1 ARP1420 stability margin definition 27
Figure 2 Fan map to illustrate stability margin definition 29
Figure 3 Fan map to illustrate effect of stability limit line extrapolation 33
Figure 4 Ring circumferential distortion for a one-per-rev pattern 35
Figure 5 Ring circumferential distortion for a multiple-per-rev pattern 36
Figure 6 Radial distortion pattern 38
Figure 7 Example of inlet pattern 39
Figure 8 Sample pattern definition and results 40
Figure 9 Circumferential distortion elements for inner ring 40
Figure 10 Circumferential distortion elements for outer ring 41
Figure 11 Radial distortion elements 41
Figure 12 Distortion-descriptor elements for the example inlet pattern 42
Figure 13 Equivalent one-per-rev pattern 42
Figure 14 180 degrees 1/rev circumferential distortion pattern 43
Figure 15 Hub-radial distortion pattern 44
Figure 16 Tip-radial distortion pattern 45
Figure 17 180 degrees 1/rev + hub-radial combined distortion pattern 46
Figure 18 180 degrees 1/rev + tip-radial combined distortion pattern 47
Figure 19 90 degrees 1/rev + tip-radial combined distortion pattern 48
Figure 20 Two/rev with lows closer than 25 degrees and with tip-radial distortion pattern 49
Figure 21 Two/rev with lows further apart than 25 degrees and with tip-radial distortion pattern 50
Figure 22 Aircraft pattern 51
Figure 23 Basic equation for calculating stability pressure ratio loss (ΔPRS) 52
Figure 24 Example of expanded circumferential sensitivity 53
Figure 25 Circumferential sensitivity 56
Figure 26 Radial sensitivity 56
Figure 27 Hub-radial offset 57
Figure 28 Tip-radial offset 57
Figure 29 Example of radial distortion data 58
Figure 30 Radial sensitivity evaluation 58
Figure 31 Constant term 59
Figure 32 Modeling radial distortion 59
Figure 33 Loss of stability pressure ratio due to 180 degrees 1/rev total-pressure distortion 64
Figure 34 One/rev total-pressure distortion sensitivity 64
Figure 35 Loss of stability pressure ratio due to hub- and tip-radial total-pressure distortion 65
Figure 36 Hub-radial total-pressure distortion sensitivity as a function of speed 66
Figure 37 Tip-radial-distortion logic guide as a function of speed 66
Figure 38 Tip-radial distortion sensitivity coefficients as a function of speed 67
Figure 39 Combined circumferential and radial total-pressure distortion superposition factors as a function of speed 68
Figure 40 1/rev total-pressure distortion angular extent function 69
Figure 41 Circumferential total-pressure distortion transfer coefficient 71
Figure 42 Circumferential total-temperature distortion generation coefficient due to total-pressure distortion 72
Figure 43 Radial total-pressure distortion 72
Figure 44 Radial total-temperature distortion due to radial total-pressure distortion 73
Figure 45 Effect of radial distortion on a fan designed for a tip-radial profile 76
Figure 46 Effect of radial distortion on a fan designed for a hub-radial profile 77
Figure 47 ΔPRS correlation of J85 data 79
Figure 48 ΔPRS correlation of a research fan 79
Figure 49 ΔPRS correlation of F101 fan 80
Figure 50 ΔPRS correlation of J58 compressor 80
Figure 51 ΔPRS correlation of a turbofan compressor 81
Figure 52 ΔPRS correlation of a turbofan core 81
Figure 53 ΔPRS correlation of F100 fan 82
Figure 54 ΔPRS correlation of TF41 fan and compressor 82
Figure 55 Stability limit line loss versus instantaneous spatial distortion 85
Figure 56 Typical compressor destabilizing factors7 88
Figure 57 Stability assessment process 90
Figure 58 Fan stability assessment example 91

AVA Documents Document Sharing Hub
Full document details: SAE AIR1419D

Figure 59 Distortion stability assessment 94
Figure 60 Example of one-per-rev square wave circumferential total-pressure distortion 95
Figure 61 Example of one-per-rev circumferential total-pressure distortion, 90 degrees extent 95
Figure 62 Example of one-per-rev circumferential total-pressure distortion, 180 degrees extent 96
Figure 63 Example of one-per-rev circumferential total-pressure distortion, 45 degrees extent 96
Figure 64 Example of one-per-rev circumferential total-pressure distortion, 22 degrees extent 97
Figure 65 Example of two-per-rev circumferential total-pressure distortion 97
Figure 66 Compressor sensitivity to one-per-rev circumferential total-pressure distortion 98
Figure 67 Example of hub-radial total-pressure distortion 99
Figure 68 Example of hub-radial total-pressure distortion, narrow extent 100
Figure 69 Example of hub-radial total-pressure distortion, wide extent 100
Figure 70 Example of mid-span-radial total-pressure distortion 101
Figure 71 Example of tip-radial total-pressure distortion, narrow extent 101
Figure 72 Example of tip-radial total-pressure distortion, wide extent 102
Figure 73 Example of combined hub-radial and circumferential total-pressure distortion 103
Figure 74 Example of combined tip-radial and circumferential total-pressure distortion 103
Figure 75 Comparison of distortion stability assessment with flight test results for fixed throttle 104
Figure 76 Comparison of distortion stability assessment with flight test results for snap-throttle transients - no surges 104
Figure 77 Supersonic, two-dimensional, external-compression inlet, Mach 2.0, cruise incidence, fixed ramps 106
Figure 78 Supersonic, two-dimensional, external-compression inlet, distortion characteristics during low-speed operation 107
Figure 79 Short subsonic bifurcated inlet 108
Figure 80 Effect of classical circumferential inlet distortion patterns 111
Figure 81 Rig compressor tests - classical distortion 112
Figure 82 Rig compressor tests - radial and mixed distortion 113
Figure 83 Rig compressor tests - screen simulated distortion 114
Figure 84 Simulated inlet-distortion screen #1 115
Figure 85 Distortion effects on three-stage fan compression 116
Figure 86 Turbofan engine performance with inlet distortion 117
Figure 87 Turbofan engine with classical circumferential distortion pattern 118
Figure 88 Turbofan engine performance with distortion 119
Figure 89 Simulated inlet-distortion screen #2 120
Figure 90 Turbofan engine performance—screen position effect 121
Figure 91 Effect of engine sensor location 122
Figure 92 Installed engine performance assessment guideline 124
Figure 93 Split-flow AIP distortion analysis example 126
Figure 94 Steady-state performance assessment with inlet distortion 129
Figure 95 Distortion assessment uncertainty during propulsion system life cycle 131
Figure 96 Subsonic diffuser model for investigating internal performance 134
Figure 97 Inlet/forebody wind tunnel model 135
Figure 98 Inlet drag wind tunnel model 136
Figure 99 0.176-scale F-18E/F model used for inlet verification tests 137
Figure 100 Compressor map showing boundaries of four types of flutter 139
Figure 101 Single-spool compressor facility 140
Figure 102 Dual-exhaust, dual-spool compressor facility 140
Figure 103 Dual-discharge compressor flowpath 141
Figure 104 Typical direct-connect engine test installation for baseline stability and performance testing 141
Figure 105 Typical classical and aircraft pattern distortion screens 142
Figure 106 Rotatable distortion screen assembly 143
Figure 107 Schematic of airjet distortion generator 144
Figure 108 Compressor rig test with airjet distortion generator installed 145
Figure 109 Test configuration for temperature distortion testing 145
Figure 110 Typical random frequency generator test installation for engine stability assessment 147
Figure 111 Random frequency generator designed to simulate flow conditions of two-dimensional inlet configuration 148
Figure 112 Typical engine test results obtained with a random frequency generator 149
Figure 113 Schematic of planar pressure pulse generator 150
Figure 114 Peebles crosswind facility 152

AVA Documents Document Sharing Hub

Full document details: SAE AIR1419D

Figure 115 Free-jet propulsion-system test installation schematic 153
Figure 116 Propulsion-system test installation in propulsion wind tunnel 153
Figure 117 Schematic of inlet simulator 154
Figure 118 Typical test data base/test matrix requirements for stability assessment verification 156
Figure 119 Stability assessment test verification methodology 157
Figure 120 Test procedure to demonstrate available margin 157
Figure 121 Schematic of test hardware for simultaneous loading of fan and gas generator hardware 158
Figure 122 Compressor operating characteristics during compressor loading operations 159
Figure 123 Engine and environmental condition criteria for test verification of stability assessments 160
Figure 124 Screen changer assembly 161
Figure 125A External force balance system 162
Figure 125B Internal force balance system 162
Figure 125 Engine thrust measurement techniques in ground test facilities 162
Figure 126 AIP instrumentation integral with IGVS 164
Figure 127 AIP instrumentation mounted on aircraft rakes just forward of IGV leading edge 165
Figure 128 AIP instrumentation mounted on aircraft rakes installed upstream of the bullet nose 166
Figure 129 Typical 40-probe/rake arrangement 167
Figure 130 Distortion factor dependence on probe/rake configuration 169
Figure 131 Full span non-IGV engine inlet rakes 171
Figure 132 Compressor face rake 172
Figure 133 F-15 rake configuration 173
Figure 134 Sketch illustrating the effect of probe size 175
Figure 135 Effect of transducer diameter 175
Figure 136 Frequency below which at least 90% of spectral function is sensed 176
Figure 137 NASA Dryden Flight Research Center rake 178
Figure 138 B-1 flight test data acquisition system 179
Figure 139 Double probe rake configuration 180
Figure 140 Development of composite signal from low- and high-response signals 181
Figure 141 Typical data acquisition system 183
Figure 142 AIP data editing technique 185
Figure 143 Generalized data fill procedure 187
Figure 144 Sequential sampling characteristics and interpolation procedures 188
Figure 145 Attenuation characteristics of Lagrange interpolation techniques 189
Figure 146 Digital time averaging filter characteristics, 2000 samples per second 191
Figure 147 Data filtering characteristics 192
Figure 148 Comparison of analog and digital PSD 194
Figure 149 Typical AIP total-pressure PSD variation with engine corrected speed 195
Figure 150 Coherence analysis for two near-field sets of probes 196
Figure 151 Coherence analysis for two far-field sets of probes 196
Figure 152 Amplitude probability density 197
Figure 153 Representative AIP total-pressure signal during ground tests with varying inlet throat height 198
Figure 154 Time histories of individual AIP (low frequency) probes and computed parameters during engine stall 199
Figure 155 Distortion time history 199
Figure 156 Typical AIP pressure contour plots 201
Figure 157 Dynamic variations in circumferential and radial distortion components 202
Figure 158 Meanline theory in terms of velocity diagrams 204
Figure 159 Streamline Curvature Code computational grid 205
Figure 160 Control volume technique 206
Figure 161 Parallel compressor theory concept 208
Figure 162 3D Euler technique approach 209
Figure 163 Typical CFD grid and results with inlet distortion (Reference 2.2.67) 210
Figure 164 A-10 hot gas ingestion during Gatling gun firing 211
Figure 165 F-15 during rocket firing 212
Figure 166 Joint strike fighter vertical landing 212
Figure 167 Categorization of inlet data 213
Figure 168 Example of tornado side inlets generating opposite bulk swirl due to a lower lip separation 214
Figure 169 Instability boundaries as influenced by pressure distortion 217
Figure 170 Typical damage caused by HCF 217
Figure 171 Non-Contact Stress Measuring System (NSMS) schematic 218

AVA Documents Document Sharing Hub

Full document details: SAE AIR1419D

Figure 172 Compressor surge—axially oscillating flow 218
Figure 173 Compressor rotating stall—circumferentially non-uniform flow 219
Figure 174 Examples of ice formation on aerodynamic surfaces 221
Figure 175 Carrier launched aircraft with steam ingestion 222

Table 1 Distortion assessment uses during the propulsion system life cycle 4
Table 2 Recommended stability margin definitions 31
Table 3 Comparison of stability margin definitions show different distortion accounting levels 31
Table 4 Effect of stability limit line extrapolation on stability accounting 33
Table 5 Methodology screens and coefficient determination 63
Table 6 Stability assessment factors 87
Table 7 Fan stability-pressure-ratio loss coefficients 91
Table 8 Fan stability margin assessment 92
Table 9 Typical stability margin assessment 93
Table 10 Classical circumferential screens 112
Table 11 Radial and mixed screens 113
Table 12 Operational conditions 124
Table 13 Turbofan thrust loss synthesis 127
Table 14 Inlet and aircraft component tests 133
Table 15 Engine component and engine tests 138
Table 16 Propulsion system tests 151
Table 17 Flight test conditions 155
Table 18 ARP1420 guidelines for location of the AIP 163
Table 19 Data scaling guidelines: Strouhal number constant (same Reynolds number and Mach number) 182

Documents
Document Sharing Hub
Full document details: SAE AIR1419D

1. SCOPE

This SAE Aerospace Information Report (AIR) addresses many of the significant issues associated with effects of inlet total-pressure distortion on turbine-engine performance and stability. It provides a review of the development of techniques used to assess engine stability margins in the presence of inlet total-pressure distortion. Specific performance and stability issues that are covered by this document include total-pressure recovery and turbulence effects and steady and dynamic inlet total-pressure distortion.

1.1 Purpose

The purpose of this document is to provide specific information about determining the effects of inlet total-pressure distortion on turbine-engine performance and stability. Testing methodologies and computational fluid dynamics (CFD) approaches are described. Types and scales of testing hardware are discussed with applications for each.

2. REFERENCES

2.1 Applicable Documents

The following publications form a part of this document to the extent specified herein. The latest issue of SAE publications shall apply. The applicable issue of other publications shall be the issue in effect on the date of the purchase order. In the event of conflict between the text of this document and references cited herein, the text of this document takes precedence. Nothing in this document, however, supersedes applicable laws and regulations unless a specific exemption has been obtained.

2.1.1 SAE Publications

Available from SAE International, 400 Commonwealth Drive, Warrendale, PA 15096-0001, Tel: 877-606-7323 (inside USA and Canada) or +1 724-776-4970 (outside USA), www.sae.org.

AIR5396 Characterizations of Aircraft Icing Conditions

AIR5656 Statistical Stability Assessment

AIR5686 A Methodology for Assessing Inlet Swirl Distortion

AIR5687 Inlet/Engine Compatibility - From Model to Full Scale Development

AIR5826 Distortion Synthesis/Estimation Techniques

AIR5866 An Assessment of Planar Waves

ARP246 Orientation of Engine Axis, Coordinate and Numbering Systems for Aircraft Gas Turbine Engines

ARP1210 Gas Turbine Engine Interface Test Data Reduction Computer Programs

ARP1420 Gas Turbine Engine Inlet Flow Distortion Guidelines

AS681 Gas Turbine Engine Performance Presentation for Computer Programs

AS755 Aircraft Propulsion System Performance Station Designation and Nomenclature

Cotter, H., "Integration of Inlet and Engine - An Engine Man’s Point of View," SAE Technical Paper 680286, 1968, https://doi.org/10.4271/680286.

Kimzey, W. and Ellis, S., "Supersonic Inlet Simulator - A Tool for Simulation of Realistic Engine Entry Flow Conditions," SAE Technical Paper 740824, 1974, https://doi.org/10.4271/740824.

Documents
Document Sharing Hub
Full document details: SAE AIR1419D

2.2 Applicable References

2.2.1 Brimelow, B. and Steenken, W.G., “Compatibility Technology Requirements, Proceedings of the Project Squid Workshop on Engine-Airframe Integration - Short Haul Aircraft,” Purdue University, Report No. PU-R1-78, May 1977.

2.2.2 Braithwaite, W.M., Graber, E.J., Jr., and Mehalic, C.M., “The Effect of Inlet Temperature and Pressure Distortion on Turbojet Performance,” AIAA 73-1316, November 1973.

2.2.3 Brimelow, B., Collins, T.P., and Pfefferkorn, G.A., “Engine Testing in a Dynamic Environment,” AIAA 74-1198, October 1974.

2.2.4 Plourde, G.A. and Brimelow, B., “Pressure Fluctuations Cause Compressor Instability,” Proceedings of the Air Force Airframe-Propulsion Compatibility Symposium, AD0876608, June 1970.

2.2.5 Calogeras, J.E., Mehalic, C.M., and Burstadt, P.L., “Experimental Investigation of the Effect of Screen Induced Total Pressure Distortion on Turbojet Stall Margin,” NASA-TM-X-2239, March 1971.

2.2.6 Williams, D.D. and Yost, J.O., “Some Aspects of Inlet/Engine Flow Compatibility,” Aeronautical Journal, September 1973.

2.2.7 Gray, W.G., “Propulsion System Flow Stability Program (Dynamic),” AFAPL-TR-68-142, Part IV, December 1968.

2.2.8 Reynolds, G.G., Vier, W.F., and Collins, T.P., “An Experimental Evaluation of Unsteady Flow Effects on an Axial Compressor - P^3 Generator Program,” AD0767615, July 1973.

2.2.9 Hodder, B.K., “An Investigation of Engine Influence on Inlet Performance,” NASA-CR-166136, January 1981.

2.2.10 Johnson, R.H., “Inlet Distortion Scaling of Wind Tunnel Model Results,” NASA-CR-143840, December 1976.

2.2.11 Spong, E.D., Hammock, M.S., and Stevens, C.H., “F-15 Inlet/Engine Test Techniques and Distortion Methodology Studies,” Volume I, Technical Discussion, NASA-CR-144866, June 1978.

2.2.12 Johnson, R.H., “Comparison of Inlet Distortion from Flight and Wind Tunnel Tests,” NASA-CR-144864, April 1978.

2.2.13 MacMiller, C.J., “Investigation of Subsonic Duct Distortion,” AD0859930, March 1969.

2.2.14 Armstrong, E.K. and Williams, D.D., “Some Intake Flow Maldistribution Effects on Compressor Rotor Blade Vibration,” Journal of Sound and Vibration, Vol. 3, pp. 349-354, May 1966.

2.2.15 Danforth, C.E., “Distortion Induced Vibration in Fan and Compressor Blading,” AIAA-1974-232, January 1974.

2.2.16 Sisto, F., “Aeromechanical Response,” AGARD Lecture Series No. 72 on Distortion Induced Engine Stability, AGARD-LS-72, Paper No. 4, October 1974.

2.2.17 Mikolojczak, A.A., Arnoldi, R.A., Snyder, L.E., and Stargardter, H., “Advances in Fan and Compressor Blade Flutter Analysis and Predictions,” Journal of Aircraft, Vol. 12, pp. 325-332, April 1975.

2.2.18 Huffman, G.D., Ostdiek, F.R., and Rivir, R.B., “An Assessment of Flow Quality Requirements for the Compressor Research Facility,” ADA023888, January 1976.

2.2.19 Overall, B.W. and Harper, R.E., “The Air Jet Distortion Generator System - A New Tool for Aircraft Turbine Engine Testing,” AIAA 77-993, July 1977.

2.2.20 Korn, J.A. and McKain, T.F., “Exploratory Research into Turbofan Stability Performance,” Vol. I and II, AD0771073 and AD0771074, November 1973.

2.2.21 Braithwaite, W.M., Dicus, J.H., and Moss, J.E., Jr., “Evaluation with a Turbofan Engine of Air Jets as a Steady-State Inlet Flow Distortion Device,” NASA-TM-X-1955, January 1970.

Documents Document Sharing Hub

Full document details: SAE AIR1419D

2.2.22 Collins, T.P., “The Aerothermodynamics of Aircraft Gas Turbine Engines: Engine Stability Considerations,” Oates, G. C., Editor, ADA059784, pp. 23-1 to 23-9, July 1978.

2.2.23 Ogorodnikov, D.A. and Yanchuck, V.A., “Investigation of Flow Pattern Simulation at Supersonic Flight Speed,” International Symposium of Air Breathing Engines, March 1976.

2.2.24 Lazalier, G.R. and Tate, J.T., “Development of a Prototype Discrete Frequency, Total Pressure Fluctuation Generator for Jet Engine/Inlet Compatibility Investigation,” Proceedings of the Air Force Airframe-Propulsion Compatibility Symposium, AD0876608, June 1970.

2.2.25 Crites, R.C. and Heckert, M.V., “Application of Random Data Techniques to Aircraft Inlet Diagnostics,” AIAA 70-597, May 1970.

2.2.26 Schweikard, W.G., “Test Techniques, Instrumentation, and Data Processing,” AGARD Lecture Series No. 72 on Distortion Induced Engine Stability, AGARD-LS-72 Paper No. 6, October 1974.

2.2.27 Motycka, D.L., “Ground Vortex - Limit to Engine/Reverser Operation,” Transactions of ASME, Journal of Engineering for Power, April 1976.

2.2.28 Billig, L.O., “Integrated Propulsion Control System (IPCS) Final Report,” ADA032439, ADA033774, ADA034172, and ADA033062, August 1976.

2.2.29 Steenken, W.G., “Effect of Transducer Diameter on Resolution of Total Pressure Fluctuations in Turbulent Flow,” Progress in Astronautics and Aeronautics, Volume 34, Instrumentation for Airbreathing Propulsion, 1974.

2.2.30 G Systems Inc., “Using LabVIEW Real-Time and Dynamic Signal Acquisition (DSA) for Propulsion Inlet Flow Distortion Pattern Assessment in Jet Engine Inlets,” 2003.

2.2.31 Holzman, J.K. and Payne, G., “Design and Flight Testing of a Nullable Compressor Face Rake,” NASA-TN-D-7162, January 1973.

2.2.32 Arend, D.J. and Saunders, J.D., “An Experimental Evaluation of the Performance of Two Combined Pitot Pressure Probes,” AIAA 2009-1073, January 2009.

2.2.33 Malloy, D.J. and Minter, M.J., “New and Improved Test Technologies to Validate and Analyze High-Response Aerodynamic Test Data,” AIAA 2008-1628, February 2008.

2.2.34 Shepard, D., “A Two-Dimensional Interpolation Function for Irregularly-Spaced Data,” Proceedings of the 1968 23rd ACM National Conference, pp. 517-524, January 1968.

2.2.35 Oates, G.C., “Aircraft Propulsion Systems Technology and Design,” AIAA, 1989.

2.2.36 Kostin, L.C. and Millstone, S.D., “Application of Statistical Parameters in Defining Inlet Airflow Dynamics,” AIAA-68-649, June 1968.

2.2.37 Cohen, H., Rogers, G.F.C., and Saravanamuttoo, H.I.H., “Gas Turbine Theory,” Longman, Third Edition, 1987.

2.2.38 Johnsen, I.A. and Bullock, R.O., “Aerodynamic Design of Axial-Flow Compressors,” NASA SP-36, 1965.

2.2.39 Tesch, W.A., Moszee, R.H., and Steenken, W.G., “Linearized Blade Row Compression Component Model: Stability and Frequency Response Analysis of a J85-13 Compressor,” NASA-CR-135162, Sept. 1976.

2.2.40 Cumpsty, N.A, “Compressor Aerodynamics,” Longman Scientific and Technical, 1989.

2.2.41 Hearsey, R.M., “HTO300 - A Computer Program for the Design and Analysis of Axial Turbomachinery,” 1970.

2.2.42 Boyer, K.M. and O’Brien, W.F., “An Improved Streamline Curvature Approach for Off-Design Analysis of Transonic Axial Compression Systems,” Transactions of the ASME, Journal of Turbomachinery, Vol. 125, pp. 475-481, July 2003.

AVA Documents
Document Sharing Hub

Full document details: SAE AIR1419D

2.2.43 Greitzer, E.M., “Surge and Rotating Stall in Axial Flow Compressors, Part I: Theoretical Compression System Model,” ASME Journal of Engineering for Power, Vol. 98, pp. 190-198, April 1976.

2.2.44 Greitzer, E.M., “Surge and Rotating Stall in Axial Flow Compressors, Part II: Experimental Results and Comparisons with Theory,” ASME Journal of Engineering for Power, Vol. 98, pp. 199-217, April 1976.

2.2.45 Hale, A.A. and Davis, M.W., Jr., “DYNamic Turbine Engine Compressor Code (DYNTECC) - Theory and Capabilities,” AIAA-92-3190, July 1992.

2.2.46 Reynolds, G.G. and Steenken, W.G., “Dynamic Digital Blade Row Compression Component Stability Model: Model Validation and Analysis of Planar Pressure Pulse Generator and Two-Stage Fan Test Data,” AFAPL-TR-76-76, August 1976.

2.2.47 Hosney, W.M., Bitter, S.J., and Steenken, W.G., “Turbofan Engine Non-Recoverable Stall Computer Simulation Development and Validation,” AIAA-85-1432, July 1985.

2.2.48 Ward, G.G., “Compressor Stability Assessment Program (Techniques for Constructing Mathematical Models of Compression Systems and Propulsion Systems),” Air Force Aero Propulsion Laboratory, TR-74-107, Vol. II, Wright-Patterson Air Force Base, OH, December 1974.

2.2.49 Davis, M.W., Jr., “A Stage-by-Stage Dual-Spool Compression System Modeling Technique,” ASME 82-GT-189, March 1982.

2.2.50 Hosney, W.M. and Steenken, W.G., “Aerodynamic Instability Performance of an Advanced High-Pressure-Ratio Compression Component,” AIAA-86-1619, June 1986.

2.2.51 Mazzawy, R.S., “Multiple Segment Parallel Compressor Model for Circumferential Flow Distortion,” Transactions of the ASME, Journal of Engineering for Power, pp. 288-296, April 1977.

2.2.52 Tesch, W.A. and Steenken, W.G., “Blade Row Dynamic Digital Compressor Program, Vol. 1, J85, Clean Inlet Flow and Parallel Compressor Models,” NASA CR-134978, March 1976.

2.2.53 Longley, J.P. and Greitzer, E.M., “Inlet Distortion Effects in Aircraft Propulsion System Integration,” AGARD-LS-183, Advisory Group for Aerospace Research & Development Lecture Series, May 1992.

2.2.54 Shahrohki, K.A. and Davis, Jr., M.W., “Application of a Modified Dynamic Compression System Model to a Low-Aspect Ratio Fan: Effects of Inlet Distortion,” AIAA-95-0301, January 1995.

2.2.55 Davis, M.W., Jr., “Parametric Investigation into the Combined Effects of Pressure and Temperature Distortion on Compression System Stability,” AIAA-91-1895, June 1991.

2.2.56 Cousins, W.T., et al., “Inlet Distortion Testing and Analysis of a High-Bypass Ratio Turbofan Engine,” Presented at the 16th International Symposium on Air Breathing Engines, ISABE-2003-1110, August 2003.

2.2.57 Hynes, T.P. and Greitzer, E.M., “A Method for Assessing Effects of Inlet Flow Distortion on Compressor Stability,” Transactions of the ASME, Journal of Turbomachinery, Vol. 109, pp. 371-379, 1987.

2.2.58 Davis, M. and Hale, A., “A Parametric Study on the Effects of Inlet Swirl on Compression System Performance and Operability Using Numerical Simulations,” GT2007-27033, May 2007.

2.2.59 Davis, M., Jr., Beale, D., and Sheoran, Y.i, “Integrated Test and Evaluation Techniques as Applied to an Inlet Swirl Investigation Using the F109 Gas Turbine Engine,” GT2008-50074, June 2008.

2.2.60 Bouldin, B. and Sheoran, Y., “Impact of Complex Swirl Patterns on Compressor Performance and Operability Using Parallel Compressor Analysis,” ISABE2007-1140, September 2007.

2.2.61 Hale, A.A. and O’Brien, W.F., “A Three-Dimensional Turbine Engine Analysis Compressor Code (TEACC) for Steady-State Inlet Distortion,” Transactions of the ASME, Journal of Turbomachinery, Vol. 120, pp. 422-430, July 1998.

AVA Documents
Document Sharing Hub

Full document details: SAE AIR1419D

2.2.62 Gong, Y., Tan, C., Gordon, K.A., and Greitzer, E.M., “A Computational Model for Short-Wavelength Stall Inception and Development in Multistage Compressors,” Transactions of the ASME, Journal of Turbomachinery, Vol. 121, pp. 726-734, October 1999.

2.2.63 Chima, R.. “A Three-Dimensional Unsteady CFD Model of Compressor Stability,” ASME GT2006-90040, May 2006.

2.2.64 Davis, M., Hale, A., and Beale, D., “An Argument for Enhancement of the Current Inlet Distortion Ground Test Practice for Aircraft Gas Turbine Engines,” Transactions of the ASME, Journal of Turbomachinery, pp. 235-241, April 2002.

2.2.65 Hale, A., Davis, M., and Sirbaugh, J., “A Numerical Simulation Capability for Analysis of Aircraft Inlet-Engine Compatibility,” Journal of Engineering for Gas Turbines and Power, Vol. 128, pp. 473-481, July 2006.

2.2.66 Yao, J., Gorrell, S.E., and Wadia, A.R., “High-Fidelity Numerical Analysis of Per-Rev-Type Inlet Distortion Transfer in Multistage Fans - Part I: Simulations with Selected Blade Rows,” ASME GT2008-50812, June 2008.

2.2.67 Yao, J., Gorrell, S.E., and Wadia, A.R., “High-Fidelity Numerical Analysis of Per-Rev-Type Inlet Distortion Transfer in Multistage Fans - Part II: Entire Component Simulation and Investigation,” ASME GT2008-50813, June 2008.

2.2.68 Wallner, L.E., Useller, J.W., and Saari, M.J., “A Study of Temperature Transients at the Inlet of a Turbojet Engine,” NACA RM E57C22, June 1957.

2.2.69 DiPietro, A.L., Jr. and O’Brien, W.F., “Design and Experimental Evaluation of a Dynamic Thermal Distortion Generator for Turbomachinery Research,” AIAA 94-0149, January 1994.

2.2.70 Aini, Y., deLaneuville, R., Stoner, A., and Capece, V., “High Cycle Fatigue of Turbomachinery Components - Industry Perspective,” AIAA-1997-3365, July 1997.

2.2.71 Manwaring, S., Rabe, D., Lorence, C., and Wadia, A., “Inlet Distortion Generated Forced Response of a Low-Aspect-Ratio, Transonic Fan,” Journal of Turbomachinery, Vol. 119, pp. 665-676, October 1997.

2.2.72 Hamed, A. and Numbers, K., “Inlet Distortion Considerations for High Cycle Fatigue in Gas Turbine Engines,” AIAA-1997-3364, July 1997.

2.2.73 Jones, H., “Development of a Noninterference Technique for Measuring Turbine Engine Rotor Blade Stresses,” AIAA-1985-1472, July 1985.

2.2.74 Chi, R. and Jones, H., “Demonstration Testing of a Noninterference Technique for Measuring Turbine Engine Rotor Blade Stresses,” AIAA-1988-3143, July 1988.

2.2.75 Vining, C., Arnold, S., Hayes, B., and Howard, R., “PC-Based Generation 4 Non-Contact Stress Measurement System,” Proceedings of the 10th National Turbine Engine High-Cycle Fatigue Conference, March 2005.

2.2.76 Emmons, H.W., Pearson, C.E., and Grant, H.P., “Compressor Surge and Stall Propagation,” Transactions of the ASME, Vol. 77, No. 4, pp. 455-467, May 1955.

2.2.77 Day, I.J., and Cumpsty, N.A., “The Measurement and Interpretation of Flow within Rotating Stall Cells in Axial Compressors,” Journal of Mechanical Engineering Sciences, The Institution of Mechanical Engineers, Vol. 20, No. 2, 1978.

2.2.78 Day, I.J., “Axial Compressor Stall,” Ph. D. Dissertation, Christ’s College (Cambridge University), 1976.

2.2.79 Burwell, A.E. and Patterson, G.T., “Dynamic Engine Behavior During Post Surge Operation of a Turbofan Engine,” AIAA 85-1430, July 1985.

2.2.80 Moore, F.K., “A Theory of Rotating Stall of Multistage Axial Compressors,” NASA CR-3685, July 1983.

2.2.81 Greitzer, E.M., “Review - Axial Compressor Stall Phenomena,” Journal of Fluids Engineering, Vol. 102, pp. 134-151, June 1980.

AVA Documents Document Sharing Hub

Full document details: SAE AIR1419D

2.2.82 Pampreen, R., “Compressor Surge and Stall,” Concepts ETI, Inc., ISBN 0-933283-05-9,1993.

2.2.83 Davis, M.W., Jr., “A Stage-by-Stage Post-Stall Compression System Modeling Technique: Methodology, Validation, and Application,” Ph.D. Dissertation, Virginia Polytechnic Institute and State University, December 1986.

2.2.84 Davis, M.W., Jr., “A Post-Stall Compression System Modeling Technique,” AEDC-TR-86-34, February 1987.

2.2.85 Davis, M.W., Jr., and O’Brien, W. F., “Stage-by-Stage Poststall Compression System Modeling Technique,” Journal of Propulsion and Power, Vol. 7, Number 6, pp. 997-1005, November-December 1991.

2.2.86 Owen, A.K., Mattern, D.L., and Le, K.D., “Comparisons of Rig and Engine Dynamic Events in the Compressor of an Axi-Centrifugal Turboshaft Engine,” ASME 96-GT-239, June 1996.

2.2.87 NATO, “Recommended Practices for the Assessment of the Effects of Atmospheric Water Ingestion on the Performance and Operability of Gas Turbine Engines,” Propulsion and Energetics Panel Working Group 24, Advisory Group for Aerospace Research and Development, NATO, 1995.

2.2.88 Hale, A., Klepper, J., and Hurwitz, W., “A Numerical Capability to Analyze the Effects of Water Ingestion on Compression System Performance and Operability,” ASME GT2005-68480, June 2005.

2.3 Related Publications

The following publications are provided for information purposes only and are not a required part of this SAE Aerospace Technical Report.

2.3.1 Crites, R.C., “The Philosophy of Analog Techniques Applied to the Analysis and High Speed Screening of Dynamic Data,” AIAA 70-595, May 1970.

2.3.2 Ellis, S. and Brownstein, B., “A Procedure for Estimating Maximum Time-Variant Distortion with Limited Instrumentation,” AIAA 72-1099, December 1972.

2.3.3 Jacocks, J.L. and Kneile, K.R., “Statistical Prediction of Maximum Time-Variant Inlet Distortion Levels,” AEDC-TR-74-121, January 1975.

2.3.4 Motycka, D.L., “Determination of Maximum Instantaneous Distortion Patterns from Statistical Properties of Inlet Pressure Data,” AIAA 76-705, July 1976.

2.3.5 Melick, H.C., Ybarra, A.H., and Bencze, D.R., “Estimating Maximum Instantaneous Distortion from Inlet Total Pressure RMS and PSD Measurements,” AIAA 75-1213, September 1975.

2.3.6 Chung, K., Hosny, W.M., and Steenken, W.G., “Aerodynamic Stability Analysis of NASA J85-13/Planar Pressure Pulse Generator Installation,” NASA-CR-165141, November 1980.

2.3.7 Chamblee, C.E., Davis, M.W., and Kimzey, W.F., “A Multi-Stage Axial Flow Compressor Mathematical Modeling Technique with Application to Two Current Turbofan Compression Systems,” AIAA 80-0054, January 1980.

2.3.8 Mehalic, C.M. and Lottig, R.A., “Steady-State Inlet Temperature Distortion Effects on the Stall Limits of a J85-GE-13 Turbojet Engine,” NASA-TM-X-2990, February 1974.

2.3.9 Baghdadi, S. and Lueke, J.E., “Compressor Stability Analysis,” ASME 81-WA/FE-18, November 1981.

2.3.10 Burstadt, P.L. and Wenzel, L.M., “A Method to Account for Variation of Average Compressor Inlet Pressure During Instantaneous Distortion Analysis,” AIAA 76-703, July 1976.

2.3.11 Surber, L. and Sedlock, D., “Effects of Airframe Inlet Integration on Half-Axisymmetric and Two-Dimensional Supersonic Inlet Performance,” AIAA 78-960, July 1978.

2.3.12 Stock, C.P. and Bissinger, N.C., “The Design and Development of the Tornado Engine Air Intakes,” AGARD Fluid Dynamics Symposium on Aerodynamics of Power Plant Installation, Paper No. 10, May 1981.

AVA Documents Document Sharing Hub

Full document details: SAE AIR1419D

2.3.13 Mitchell, G.A., “Effect of Inlet Ingestion of a Wing Tip Vortex on Turbojet Stall Margin,” NASA-TM-X-71610, September 1974.

2.3.14 Motycka, D.L. and Walter, W.A., “An Experimental Investigation of Ground Vortex Formation During Reverse Engine Operation,” AIAA 75-1322, October 1975.

2.3.15 Wallace, R., Kenyon, J., King, P., and O’Brien, W., “Assessing Fan and Compressor Blade HCF Sensitivity to Non-Uniform Inlet Flows,” ASME GT2004-54264, June 2004.

2.3.16 Longley, J.P., Shin, H.-W., Plumley, R.E., Silkowski, P.D., Day, I.J., Greitzer, E.M., Tan, C.S., and Wisler, D.C., “Effects of Rotating Inlet Distortion on Multistage Compressor Stability,” Transactions of the ASME, Journal of Turbomachinery, 1996.

2.3.17 Greitzer, E.M., Mazzawy, R.S., and Fulkerson, D.A., “Flow Field Coupling Between Compression Components in Asymmetric Flow,” ASME 77-GT-17, March 1977.

2.3.18 Greitzer, E.M. and Griswold, H.R., “Coupled Compressor-Diffuser Interaction with Circumferential Flow Distortion,” Journal of Mechanical Engineering Sciences, Vol. 18, pp. 25-38, February 1976.

2.3.19 Ward, G.C., “Compressor Stability Assessment: Dual Spool Compressor System Test and Data Analysis,” AFAPL-TR-74, Vol. 1, December 1974.

2.3.20 Smith, R.E., “Marrying Airframes and Engines in Ground Test Facilities - An Evolutionary Revolution,” AIAA 95-0950, 1995 Wright Brothers Lectureship in Aeronautics, September 1995.

2.3.21 Childs, H.J., Kichendorfer, F.D., Lubick, R.J., and Friedman, R., “Stall and Flameout Resulting from Firing of Armament,” NACA RM E55E25, August 1955.

2.3.22 Welch, G.E., “Determination of Critical Sector Angle of Inlet Swirl Distortion Using Actuator-Duct Model,” AIAA-2007-5057, July 2007.

2.4 Symbols and Abbreviations

1D, 1-D	One dimensional
3D, 3-D	Three dimensional
A	Area
A/B	Afterburner
AC	Alternating current
A/C	Aircraft
A/D	Analog-to-digital
AEDC	Arnold Engineering Development Center
AGARD	Advisory Group for Aerospace Research and Development
AIP	Aerodynamic interface plane
AIR	Aerospace Information Report
AOA	Angle of attack, degrees
AOS	Sideslip angle, degrees

AVA Documents Document Sharing Hub

Full document details: SAE AIR1419D

APD	Amplitude probability density
ARP	Aerospace Recommended Practice
ASME	American Society of Mechanical Engineers
ATF	Altitude test facility
A_P	Pressure distortion transfer function
A_T	Temperature distortion transfer function
b	Stability limit line loss weighting or superposition factor
B	AIP distortion parameter weighting or superposition factor
BLC	Boundary layer control
b_p	The ratio of the loss of stability pressure ratio due to a 180 degree one-per-rev low pressure region with radial distortion to the loss of stability pressure ratio due to a pure circumferential 180 degree one-per-rev pattern
b_T	Superposition function which accounts for coupling effects between the circumferential and radial components of total-temperature distortion
CC_P	Circumferential total-pressure distortion offset coefficient for sensitivity or portion of sensitivity lines not passing through the origin
CC_T	Circumferential total-temperature distortion offset coefficient for sensitivity or portion of sensitivity lines not passing through the origin
$CDGC_p$	Distortion generation coefficient
$CDTC_p$	Distortion transfer coefficient
CFD	Computational fluid dynamics
C_h	Radial offset term for the hub
C_i	Constant (offset) for ring i
CR_p, C_R	Radial total-pressure distortion offset coefficient for sensitivity or portion of sensitivity lines not passing through the origin
CR_T	Tip radial total-pressure distortion offset coefficient for sensitivity or portion of sensitivity lines not passing through the origin; radial total-temperature distortion offset coefficient for sensitivity or portion of sensitivity lines not passing through the origin
C_t	Radial offset term for the tip
D	Diameter
DFRC	Dryden Flight Research Center

Documents
Document Sharing Hub
Full document details: SAE AIR1419D

DPC	Circumferential distortion parameter
DPR	Radial distortion parameter
DPS	AIP distortion screening parameter
DTC	Temperature distortion parameter
ECS	Environmental control system
EX_p	Extent function which accounts for change in loss of stability pressure ratio due to the extent of the total-pressure pattern differing from 180 degrees
EX_T	Extent function which accounts for change in loss of stability pressure ratio due to the extent of the total-temperature pattern differing from 180 degrees
f	Frequency
F	Force
FADEC	Full authority digital electronic control
F_g	Gross thrust
FOD	Foreign object damage
$f(\theta)$	Combined pressure and temperature distortion superposition and spatial orientation function
$f\left(\theta_i^-\right)$	Extent function
FX	Axial force distribution
g	Acceleration due to gravity
HCF	High cycle fatigue
HP	High-pressure
HPC	High-pressure compressor
ID	Inner diameter
IGV	Inlet guide vanes
I_R	Radial intensity parameter
JSF	Joint Strike Fighter
KC_i	Circumferential distortion sensitivity for ring i
KC_P	Circumferential total-pressure distortion sensitivity
KC_T	Circumferential total-temperature distortion sensitivity
K_r	Average radial sensitivity

AVA Documents Document Sharing Hub

Full document details: SAE AIR1419D

KRAD	Radial distortion factor
KR_i	Radial distortion sensitivity for ring i
KR_p	Radial total-pressure distortion sensitivity
KR_T	Tip radial total-pressure distortion sensitivity
K_T	Temperature distortion sensitivity
K_θ	Circumferential distortion factor
L	Characteristic length
LP	Low-pressure
LPC	Low-pressure compressor
LWC	Liquid water content, the mass of the supercooled liquid in a unit volume of dry air
m	Mass
M	Mach number
$\dot{m}$	Mass flux
MFR	Mass flow ratio
MLC	Meanline code
MPR	Multiple per revolution
MVD	Median volumetric diameter (half of the LWC is of greater diameter and half of the LWC is of lower diameter)
N	Number of instrumentation rings; turbine engine rpm
NACA	National Advisory Committee for Aeronautics
NAPC	Naval Air Propulsion Center
NASA	National Aeronautics and Space Administration
NATO	North Atlantic Treaty Organization
NC	Core speed, rpm
N_C	Engine rpm corrected to standard sea level conditions
NF	Fan speed, rpm
NR	Non-random
NSMS	Noninterference Stress Measuring System
OD	Outer diameter

Documents
Document Sharing Hub
Full document details: SAE AIR1419D

P	Static pressure
PAV	Average pressure, usually for a ring
P_{AVG}	Average total pressure of the AIP
PAVLOW	Average pressure in the extent
PFAV	AIP average total pressure
PLA	Power lever angle
P_{MAX}	Maximum total pressure of the AIP
P_{MIN}	Minimum total pressure of the AIP
PR1	Pressure ratio on undistorted flow stability limit line
PRDS	Distorted flow pressure ratio
PRi, PR(i), PR_i	Pressure ratio i
PRDS	Pressure ratio on distorted flow stability limit line
PRO	Pressure ratio on undistorted operating line
PSD	Power spectral density
P_t'	Relative total pressure
Q	Rate of heat added to a fluid
r	Radius
RANS	Reynolds averaged Navier-Stokes
RFG	Random frequency generator
RMS	Root mean square
rpm	Revolutions per minute
RSS	Root-sum-square
S	Superposition function which accounts for coupling effects between total-pressure distortion and total-temperature distortion
SFC	Specific fuel consumption
SLCC	Streamline curvature code
SM	Stability margin
SSA	Statistical stability assessment
S-16	SAE Turbine Engine Inlet Flow Distortion Committee

Documents
Document Sharing Hub
Full document details: SAE AIR1419D

SW	Shaft work
T	Temperature
TDC	Top dead center
TR	Total temperature ratio
U	Velocity, local wheel speed
U_C	Convective velocity
V	Velocity; absolute velocity
V_m	Axial velocity
V_R	Relative velocity
VSTOL	Vertical/Short Takeoff and Landing
V_t	Tangential velocity
WA, WA2	Compressor inlet corrected airflow
W_B	Mass transfer rate across boundary
α, AOA	Test article angle of attack; absolute air angle
α_i	Weighting factor for ring i
β, AOS	Test article angle of sideslip; relative air angle
β_{metal}	Blade metal angle
γ	Ratio of specific heats
δ	Temperature ratio; deviation
ΔPC/P	Circumferential pressure distortion intensity element
ΔP/PC	Circumferential total pressure distortion term
ΔP/PR	Radial total pressure distortion term
ΔPR/P	Radial pressure distortion intensity element
ΔPRS	Loss of stability pressure ratio
ΔPRS_C	Stability pressure ratio loss due to circumferential total pressure distortion
ΔPRS_R	Stability pressure ratio loss due to radial total pressure distortion
ΔPRS_T	Stability pressure ratio loss due to temperature distortion
ΔSL	Loss of stability limit line

Documents
Document Sharing Hub
Full document details: SAE AIR1419D

ΔSM	Loss in stability margin
ΔT/TC	Circumferential total temperature distortion term
ΔT/TR	Radial total temperature distortion term
$(\Delta T/TC)_{25}$	Level of HPC inlet circumferential total-temperature distortion
η	Efficiency
θ^-	Extent in degrees of a low-pressure region
θ^+	Extent in degrees of a high-pressure region
λ	Wavelength
ρ	Density of air
σ	One standard deviation
τ	Characteristic time or time constant
ϕ	Auto-power spectra
ω	Pressure ratio loss

Subscripts

1	Blade entrance
180	Related to a 180 degree pattern
2	Blade exit
25	Inlet/engine station 25
c	Circumferential
h	Hub
HPC	High-pressure compressor
HUB	Related to the hub
i	Ring number
p	Pressure
r	Radial
t, TIP	Related to the tip
T	Temperature
U	Associated with velocity component U
θ	Related to extent

Documents
Document Sharing Hub
Full document details: SAE AIR1419D

3. STABILITY MARGIN AND LOSS OF STABILITY PRESSURE RATIO

Compressor stability margin definitions fall into two general classes: (1) stability margin defined at constant corrected airflow, usually at the compressor inlet, and (2) stability margin defined at constant corrected rotor speed.

Stability margin defined at constant airflow has advantages for inlet-engine airflow matching and stability assessment. With this definition, both inlet distortion and engine distortion tolerance can be expressed as functions of airflow. Consequently, the corrected airflow passing through the aerodynamic interface plane can be used as the common denominator for both inlet distortion and engine distortion tolerance.

Stability margin defined at constant corrected rotor speed has advantages for the engine manufacturer as most compressor design procedures and testing are carried out at constant corrected rotor speeds. Also, stability margin at the limiting rotor speed can typically be experimentally determined without extrapolation. Some engine configurations (e.g., auxiliary power units and single spool turboprops) are designed to operate at constant mechanical speed. It often makes sense to consider completing stability margin assessments using the constant corrected speed accounting method for these engine configurations. Additionally, for compression components which exhibit flat speed-line characteristics (i.e., small pressure ratio changes with relatively large changes in corrected airflow), constant corrected speed stability margin assessments can improve the resolution of the destabilizing terms used in the assessment.

NOTE: When constant corrected speed stability accounting methods are being used, it is often necessary to provide a compressor corrected airflow versus corrected speed characteristic to the inlet design team thereby facilitating corrected airflow matching at the aerodynamic interface plane.

The inlet/engine compatibility guidelines of ARP1420 recommend a total-pressure distortion methodology which uses constant corrected airflow accounting. This section discusses that definition and the rationale for its choice. Additionally, the corresponding constant corrected speed stability accounting definitions are provided to facilitate appropriate use of that method.

3.1 ARP1420 Definitions and Rationale

ARP1420 recommends that stability margin accounting be defined using the constant corrected airflow approach with airflow defined at the inlet of the compression component. The recommended ARP1420 stability margin is calculated as the difference between the stability pressure ratio and the operating pressure ratio, normalized by the operating pressure ratio. Referring to Figure 1, the ARP1420 undistorted percent stability margin available is defined as:

$$SM = \frac{PR1 - PRO}{PRO} \times 100 \qquad \text{(Eq. 1)}$$

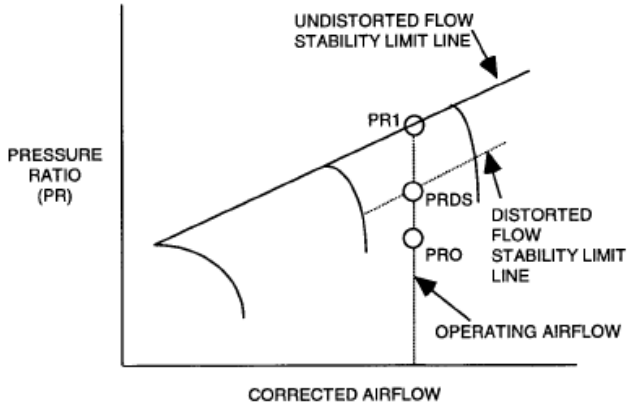


Figure 1 - ARP1420 stability margin definition

Documents
Document Sharing Hub
Full document details: SAE AIR1419D

The ARP1420 loss in stability pressure ratio due to inlet total pressure distortion (ΔPRS) also is measured at constant inlet corrected airflow with the variable geometry, if any, in the scheduled position. ΔPRS is the loss in percent stability pressure ratio due to inlet distortion normalized by the undistorted stability pressure ratio. With reference to Figure 1:

$$\Delta PRS = \frac{PR1 - PRDS}{PR1} \times 100 \qquad \text{(Eq. 2)}$$

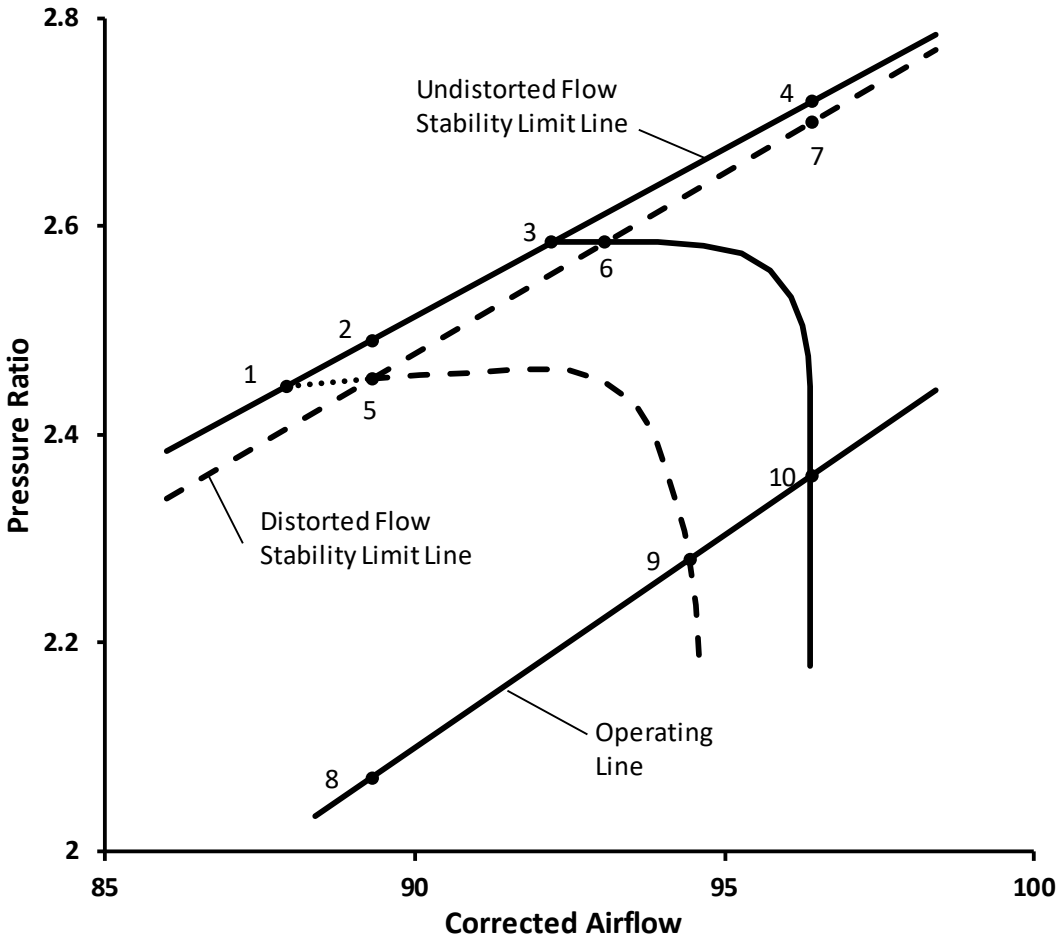
The loss in stability pressure ratio is normalized by the undistorted stability pressure ratio rather than by the operating pressure ratio because the operating pressure ratio may not have been defined when compressor rig tests were made to determine the effect of distortion on compressor stability. Also, a better comparison among compressors from different engines can be made using a distortion sensitivity that is independent of the operating point. By creating a distortion sensitivity correlation for the compression system that is independent of the operating point, the same correlation can be used in multiple engine configurations which are derived from that single unique compression system.

While stability margin at constant corrected airflow is the recommended approach for typical stability margin accounting, there are sometimes good reasons to consider conducting stability margin assessments using a constant corrected speed approach. Such an approach might be used for operating condition changes that result in small changes in compression system pressure ratio while at the same time exhibiting large changes in compressor corrected airflow along a constant corrected speed line. Engines which are routinely operated at constant mechanical speed, low-pressure-ratio fans, and some centrifugal compressors exhibit such behavior. For that reason, stability margin accounting along a constant corrected speed has become a stability margin accounting approach used by some engine manufacturers. Equations similar to those used in Equations 1 and 2 are typically used for constant corrected speed stability margin accounting.

NOTE: All margin and destabilizing factors associated with a specific operating condition in a stability margin accounting process must be consistently accounted for. That is, constant corrected airflow-based audits require that stability margin and all line item destabilizing factors must be derived from a single consistent constant corrected airflow line for the specific operating condition being evaluated, while constant corrected speed-based audits must ensure that stability margin and all line item destabilizing factors must follow the corresponding single consistent constant corrected speed line associated with the specific operating condition being evaluated. In what follows, equation designations with an "a" are associated with distortion-based constant corrected airflow stability accounting and equations designated with a "b" are associated with distortion-based constant corrected speed accounting.

Fan data, both with and without inlet distortion, are shown in Figure 2 to illustrate the definitions of stability margin and loss of stability pressure ratio due to inlet distortion.

Documents
Document Sharing Hub
Full document details: SAE AIR1419D



Point Number	Corrected Airflow	Pressure Ratio
1	87.9	2.45
2	89.3	2.49
3	92.2	2.58
4	96.4	2.72
5	89.3	2.45
6	93.1	2.58
7	96.4	2.70
8	89.3	2.07
9	94.4	2.28
10	96.4	2.36

Figure 2 - Fan map to illustrate stability margin definition

Using the nomenclature of Figure 2, ARP1420 constant corrected airflow stability margin, with no inlet distortion, at 89.3% airflow is:

$$SM = \frac{(PR)_2 - (PR)_8}{(PR)_8} \times 100 = 20.29\% \qquad \text{(Eq. 3a)}$$

Alternatively, the corresponding constant corrected speed undistorted flow stability margin is calculated as:

$$SM = \frac{(PR/WA)_1 - (PR/WA)_9}{(PR/WA)_9} \times 100 = 15.40\% \qquad \text{(Eq. 3b)}$$

Documents
Document Sharing Hub
Full document details: SAE AIR1419D

In the example shown in Figure 2, the dashed lines represent a shift in performance due to inlet distortion. The loss in stability pressure ratio at constant corrected airflow due to distortion is calculated at the stability limit airflow with inlet distortion. At 89.3% inlet airflow:

$$\Delta PRS = \frac{(PR)_2 - (PR)_5}{(PR)_2} \times 100 = 1.61\% \quad \text{(Eq. 4a)}$$

Alternatively, the equivalent distorted constant corrected speed loss of stability limit line, ΔSL, is calculated as:

$$\Delta SL = \frac{(PR/WA)_1 - (PR/WA)_5}{(PR/WA)_1} \times 100 = 1.57\% \quad \text{(Eq. 4b)}$$

With reference to Figures 1 and 2, the stability margin with distorted flow for constant corrected airflow is:

$$SM_{dist} = \frac{PRDS - PRO}{PRO} \times 100 = \frac{(PR)_5 - (PR)_8}{(PR)_8} \times 100 = 18.36\% \quad \text{(Eq. 5a)}$$

In a similar fashion, the corresponding distorted stability margin at constant corrected speed is:

$$SM_{dist} = \frac{(PR/WA)_5 - (PR/WA)_9}{(PR/WA)_9} \times 100 = 13.59\% \quad \text{(Eq. 5b)}$$

The change in stability margin at constant corrected airflow is related to the loss of stability pressure ratio, ΔPRS, by:

$$\Delta SM = \frac{PR1}{PRO}\Delta PRS = \left(\frac{(PR)_2}{(PR)_8}\right)\Delta PRS = \left(1 + \frac{SM}{100}\right)\Delta PRS \quad \text{(Eq. 6a)}$$

Similarly, the change in stability margin at constant corrected speed is related to the loss of stability limit line, ΔSL, by:

$$\Delta SM = \frac{(PR/WA)_1}{(PR/WA)_9}\Delta SL = \left(1 + \frac{SM}{100}\right)\Delta SL \quad \text{(Eq. 6b)}$$

Substituting the corresponding numerical values from this example yield for constant corrected airflow:

$$\Delta SM = \frac{2.49}{2.07}1.61 = \left(1 + \frac{20.29}{100}\right)1.61 \quad \text{(Eq. 7a)}$$

While for constant corrected speed accounting we get:

$$\Delta SM = \frac{2.45/87.9}{2.28/94.4}1.57 = \left(1 + \frac{15.40}{100}\right)1.57 \quad \text{(Eq. 7b)}$$

For the constant corrected airflow example, at 89.3% airflow:

$$\Delta SM = 1.2029 \times 1.61 = 1.93\% \quad \text{(Eq. 8a)}$$

While the corresponding constant corrected speed accounting passing through the same stability limit point yields:

$$\Delta SM = 1.1540 \times 1.57 = 1.81\% \quad \text{(Eq. 8b)}$$

Documents
Document Sharing Hub
Full document details: SAE AIR1419D

3.2 Recommended Definitions of Stability Margin

While many definitions of stability margin have been used in the past, the propulsion community has generally reached consensus on the two stability margin accounting approaches discussed and illustrated in 3.1. The current consensus stability margin definitions in terms of the nomenclature and numerical values of the undistorted flow lines in Figure 2 are provided in Table 2, illustrating that the numerical value of stability margin is dependent on the stability margin definition.

The list of stability margin definitions in Table 2 is not comprehensive and while other definitions do exist, this document recommends use of the constant corrected airflow approach to facilitate simple and effective communication between engine operability and airframe inlet design teams. As stated previously, in some circumstances there may be benefits to use constant corrected speed accounting methods and as such, the second stability margin definition is provided in Table 2.

Table 2 - Recommended stability margin definitions

Number	Definition	Percent Stability Margin	
1	$\frac{(PR)_4 - (PR)_{10}}{(PR)_{10}} \times 100$	15.25 (Refer to ARP1420)	Constant Corrected Airflow
2†	$\frac{(PR/WA)_3 - (PR/WA)_{10}}{(PR/WA)_{10}} \times 100$	14.30	Constant Corrected Speed

† WA denotes compressor inlet corrected airflow.

NOTE: For compression systems exhibiting vertical compression system corrected speed lines, the constant corrected speed accounting process decomposes into the constant corrected airflow approach and yields identical stability margin results. However, for all non-vertical speed line characteristics, care must be taken to assure that all accounting line items included in a stability audit consistently follow the constant corrected airflow approach for constant corrected airflow audits or the constant corrected speed line approach for constant corrected speed audits.

3.3 Stability Margin with Inlet Distortion

Clean-flow stability available margin, distorted-flow stability margin, and the loss in stability margin due to inlet distortion calculated for the two definitions of stability margin presented in Table 2 are compared in Table 3. Clean-flow stability margins in Table 3 range from 15.40 to 20.29%, while the corresponding loss in stability margin due to the test level of circumferential distortion ranges from 1.81 to 1.93%.

Table 3 - Comparison of stability margin definitions show different distortion accounting levels

Definition Number	Data Points		Undistorted-Flow Stability Margin, Percent	Distorted-Flow Stability Margin, Percent	Constant Corrected Airflow	Constant Corrected Speed	Loss in Stability Margin Due to Distortion, Percent
	Undistorted Flow	Distorted Flow			ΔPRS	ΔSL	
1	2, 8	5, 8	20.29	18.36	1.61	----------	1.93
2	1, 9	5, 9	15.40	13.59	----------	1.57	1.81

The effects of inlet total-pressure distortion on engine stability can be accounted for consistently using either of the compressor stability margin definitions listed above. Definitions which give higher values of stability margin usually have greater sensitivity to distortion so that all definitions reproduce the test stability limit point for the test level of inlet distortion. However, each method may estimate a different stability-limit-remaining value prior to reaching the compression system stability limit.

Rotor speed and airflow relationships are required, both with and without inlet distortion, to match inlet operating airflow for constant speed stability margin definitions. Constant airflow stability margin definitions, on the other hand, enable rapid assessments of distortion effects on stability margin to be made at the matched inlet and engine airflow. Stability assessments made at constant inlet corrected airflow, defined at the aerodynamic interface plane, simplify communication across the interface plane since inlet performance, inlet stability, inlet distortion, engine performance and engine stability are all functions of the corrected airflow at the interface plane.

AVA Documents Document Sharing Hub

Full document details: SAE AIR1419D

Different definitions of stability margin give different numerical values for stability margin and loss in stability margin, as illustrated by Table 3. This can cause confusion in inlet/engine compatibility studies because each definition provides a different numerical description of stability. Consequently, an engineer trying to compare the stability of propulsion systems that utilize different definitions of stability margin and different accounting procedures has to understand different methodologies and then translate stability margins into a common reference frame for comparison. This translation may require data that are not readily available, such as compressor maps with and without distortion. Such a translation will certainly require additional work for accurate comparison of different audit system results.

The ARP1420 constant-corrected-airflow stability-margin definition and the associated ΔPRS definition are recommended by the SAE S-16 Committee to meet the need for a consistent approach to quantifying inlet/engine stability assessment with inlet total-pressure distortion. Stability accounting systems based on these definitions are widely used and have been successful on all applications to date.

The use of the ARP1420 definition of stability margin for inlet total pressure distortion assessment does not preclude the use of alternative stability margin definitions for compressor design and development purposes. As stated in ARP1420, a particular engine configuration may require an alternative stability margin definition. In this case, the stability margin definition, stability margin loss, and stability assessment procedure need to be specified.

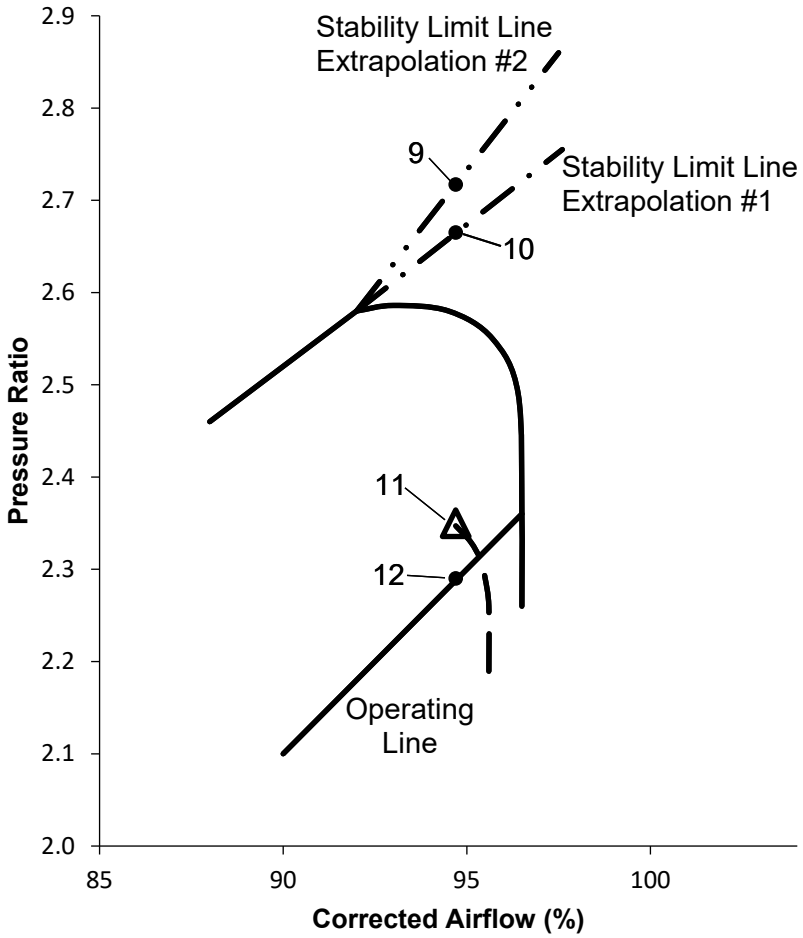
3.4 Stability Limit Line Extrapolation in the Compressor Overspeed Region

In the example of Figure 2, the stability limit line was defined up to the operating airflow by testing at higher rotor speeds on the compressor rig. In some test rig situations, the achievement of high corrected rotor speeds and corresponding airflows may not be possible. For example, rig power supply constraints may make it impossible to determine experimentally a stability limit line at high airflows in the compressor overspeed regime. If the operational limit rotor speed is achievable, extrapolation of the stability limit line still may be required to extend the stability limit line to the highest operating airflow.

It is common practice to test compression components without distortion and at one level of distortion. Linear interpolation is used to estimate the loss of stability pressure ratio due to differing inlet distortion intensities. The following example shows how different stability limit line extrapolations can affect this estimation procedure. The same undistorted speed line in Figure 2 also appears in Figure 3, but in Figure 3 it is assumed that the speed line shown is a limiting speed line. A speed line with radial distortion intensity of 0.10 also is shown in Figure 3. Stability limit line extrapolation 1 is the same stability limit line as shown in Figure 2 for undistorted operation. Stability limit line extrapolation 2 is a higher stability limit line extrapolation. The matched inlet-engine airflow has been selected as the test airflow with inlet distortion, 94.9% airflow, so that stability accounting can reproduce the test conditions.

The effect of these different stability limit line extrapolations on estimates of the ARP1420 stability margin for various levels of distortion are shown in Table 4.

Documents
Document Sharing Hub
Full document details: SAE AIR1419D



No Inlet Distortion Limiting Speed

With Radial Inlet Distortion Limiting Speed, ΔPR/P = 0.10

Point Number	Pressure Ratio	Airflow
9	2.71	94.9
10	2.67	94.9
11	2.35	94.9
12	2.30	94.9

Figure 3 - Fan map to illustrate effect of stability limit line extrapolation

Table 4 - Effect of stability limit line extrapolation on stability accounting

Inlet Distortion Level (ΔPR/P)	SM - Stability Margin with Inlet Distortion		ΔPRS - Loss in Stability Pressure Ratio Due to Inlet Distortion	
	Stability Limit Line 1	Stability Limit Line 2	Stability Limit Line 1	Stability Limit Line 2
0	16.1	17.8	0	0
0.05	9.1	10.0	6.0	6.6
0.10	2.2	2.2	12.0	13.3
0.11	0.8	0.6	13.2	14.6

Documents
Document Sharing Hub
Full document details: SAE AIR1419D

It can be seen by examining Table 4:

- A higher undistorted stability limit line is compensated by an increased loss in stability pressure ratio with inlet distortion, so that both stability limit line extrapolations produce the same distorted stability margin for the test conditions of ΔPR/P = 0.10.

- A high stability limit line extrapolation (2) gives higher stability margin estimates for distortion levels that are lower than tested and lower stability margin estimates for distortions higher than tested.

Distortion tests should be conducted at or above maximum anticipated distortion levels because interpolation is ALWAYS safer than extrapolation.

4. STABILITY PRESSURE RATIO CORRELATION

Estimation of the loss of stability pressure ratio (ΔPRS) due to inlet total-pressure distortion is fundamental to accomplishing a stability assessment (Section 5). ΔPRS, defined in Section 3, can be correlated using the distortion descriptor elements described in this section. This section also discusses the rationale underlying the selection of these distortion descriptor elements.

Sample probe readings based upon screen test data are given for a variety of patterns useful for constructing a stability pressure-ratio correlation system and for checking out a distortion descriptor element computation program. To aid this process, the data are given in terms of probe-by-probe total-pressure readings and the associated contour plot; the results are presented as descriptor element values and illustrated with bar charts.

Three correlation systems are described to familiarize the reader with the type of data required for constructing a stability pressure ratio distortion correlation system and to illustrate achievable accuracies. Section 4 ends with discussions of methods for and problems of screening inlet data and formulating a universal screening procedure.

4.1 Distortion Descriptor Element Definitions

Aerodynamic Interface Plane total-pressure probe data are used to describe inlet distortion directly in terms of the probe readings (pattern) and numerically in terms of distortion descriptors that are related to the severity of the distortion. Distortion descriptors provide a means of identifying critical distorted inlet-flow conditions and of communicating during propulsion system development. A universal distortion descriptor is beyond the state-of-the-art; however, distortion descriptor elements have been identified (refer to ARP1420) for use in structuring a distortion descriptor for a particular engine. These elements are used to define each distortion descriptor system and its associated computation procedure. The distortion descriptor elements are used to quantify the distortion at the AIP. Fundamental to the distortion-descriptor elements is the set of pressure-probe readings that are used to describe the total-pressure distribution. The pressure probes usually are arranged in rake and ring arrays, as described in Section 8. Circumferential and radial distortion elements, which are calculated using the pressure-probe readings, are defined on a ring-by-ring basis. Inlet spatial distortion is described in terms of circumferential and radial elements and is discussed in detail in the following paragraphs.

Circumferential distortion is described for each instrumentation ring in terms of intensity, extent and multiple-per-revolution elements.

Intensity: The circumferential distortion intensity element (ΔPC/P) is a numerical indication of the magnitude of the pressure defect for each ring.

Extent: The circumferential distortion extent element (θ^-) is the angular region, in degrees, in which the pressure is below ring average pressure.

Multiple-per-Revolution: The circumferential distortion multiple-per-revolution element (MPR) is a numerical indication of the “effective” number of low-pressure regions for each ring.

The radial distortion intensity element (ΔPR/P) describes the difference between the ring-average pressure and the face-average pressure for each ring. Both positive and negative values of radial intensity are possible. Positive values reflect a ring-average pressure that is below the face-average pressure.

Documents
Document Sharing Hub
Full document details: SAE AIR1419D

4.1.1 Circumferential Distortion Elements - One-Per-Rev Patterns

The “intensity” and “extent” elements of circumferential distortion are obtained by linear interpolation of the pressures in a given instrumentation ring i. Typical pressures for the probes in the i^{th} ring for a representative one-per-revolution pattern (one pressure defect in 360 degrees) are shown in Figure 4. Theta minus, θ_i^-, is the circumferential extent of the low-pressure region measured in degrees. It is defined by the intersection between the ring average pressure and the linear interpolation which subtends the low-pressure region.

$$\text{Extent} = \left(\theta^-\right)_i = \theta_{2_i} - \theta_{1_i} \quad \text{(Eq. 9)}$$

Intensity,

$$\left(\frac{\Delta PC}{P}\right)_i = \frac{(PAV)_i - (PAVLOW)_i}{(PAV)_i} \quad \text{(Eq. 10)}$$

where:

$$(PAV)_i = \frac{1}{360}\int_0^{360} P(\theta)_i \, d\theta = \text{ring i average pressure} \quad \text{(Eq. 11)}$$

$$(PAVLOW)_i = \frac{1}{\theta_i^-}\int_{\theta_i^-} P(\theta)_i d\theta \quad \text{(Eq. 12)}$$

$P(\theta)_i$ is a function resulting from a linear fit between the data points.

The intensity element is equal to the shaded area of Figure 4 divided by the product of θ_i^- times $(PAV)_i$, and:

$$\text{Multiple-Per-Rev} = (MPR)_i = 1 \quad \text{(Eq. 13)}$$

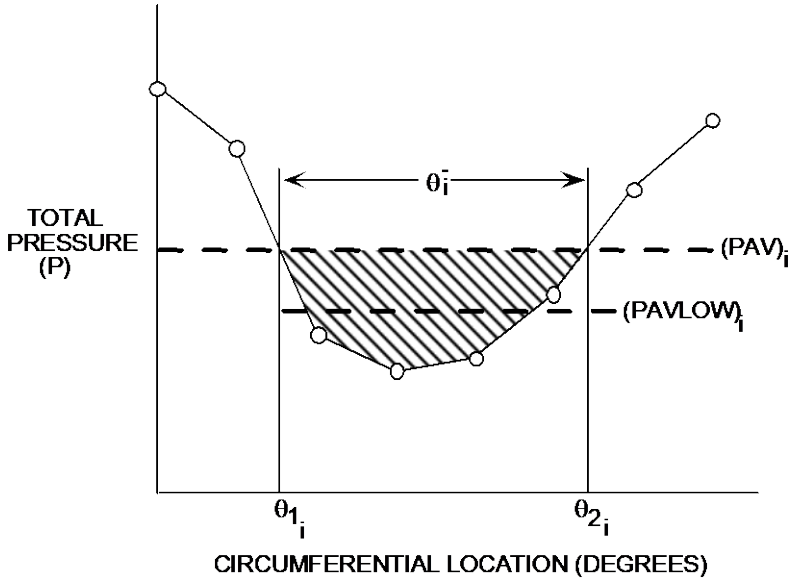


Figure 4 - Ring circumferential distortion for a one-per-rev pattern

Documents
Document Sharing Hub
Full document details: SAE AIR1419D

4.1.2 Circumferential Distortion Elements - Multiple-Per-Rev Patterns

The circumferential distortion intensity and extent elements for multi-lobe distortion patterns also are determined by a linear interpolation procedure. A pattern with two low-pressure regions separated by two high-pressure regions of extents θ_{i1}^{+} and θ_{i2}^{+} appears in Figure 5. In all that follows, the analytical expressions are written for the k^{th} low-pressure region for Q low-pressure regions for each ring. The extent and intensity elements of each low-pressure region are calculated using Equations 9 and 10.

4.1.2.1 Patterns with $\theta_{ik}^{+} \le \theta_{min}^{+}$

If the pattern has low-pressure regions circumferentially separated by high-pressure regions with extents less than or equal to θ_{min}^{+}, it is considered as an equivalent one-per-revolution low-pressure region. θ_{min}^{+} is specified by the descriptor developer and is a function of the predicted or measured engine response to distortion. A value of θ_{min}^{+} of approximately 25 degrees is suggested in the absence of other information.

In Figure 5,

$$\text{Extent} = \theta_i^{-} = \sum_{k=1}^{Q} \theta_{ik}^{-} = (\theta_2 - \theta_1)_i + (\theta_4 - \theta_3)_i \qquad \text{(Eq. 14)}$$

$$\text{Intensity} = \left(\frac{\Delta PC}{P}\right)_i = \frac{(PAV)_I - (PAVLOW)_I}{(PAV)_I} \qquad \text{(Eq. 15)}$$

where:

$$(PAVLOW)_i = \frac{1}{\theta_i^{-}} \sum_{k=1}^{Q} \int_{\theta_{ik}^{-}} P(\theta)_i \, d\theta \qquad \text{(Eq. 16)}$$

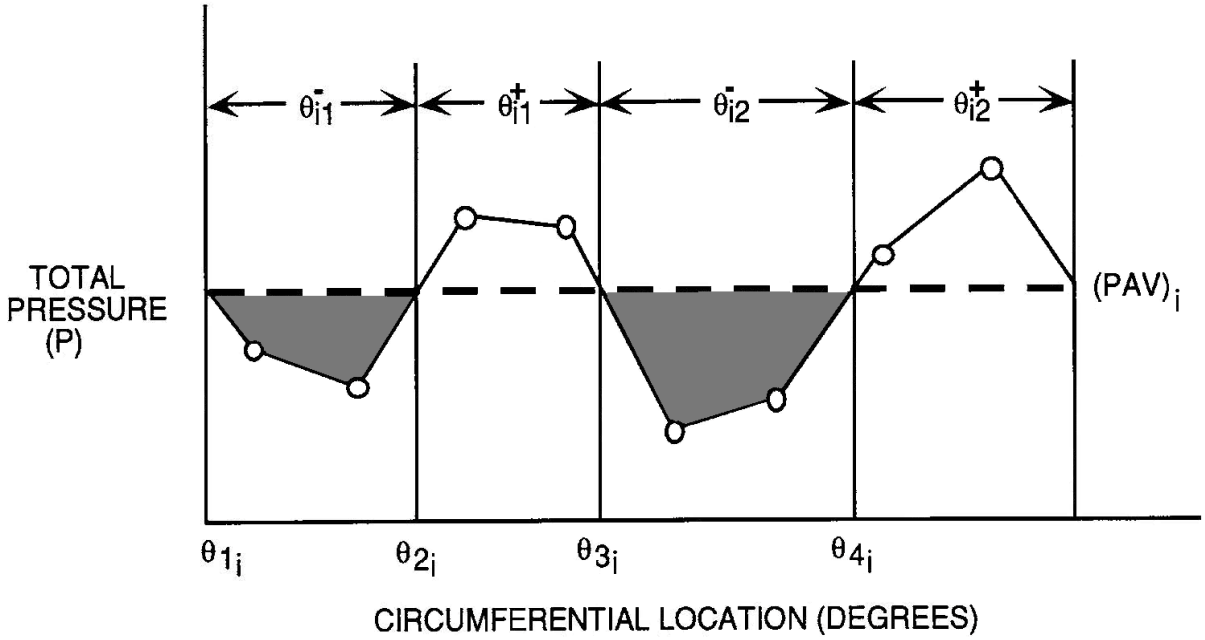


Figure 5 - Ring circumferential distortion for a multiple-per-rev pattern

Documents
Document Sharing Hub
Full document details: SAE AIR1419D

Hence,

$$\left(\frac{\Delta PC}{P}\right)_i = \frac{\sum_{k=1}^{Q}\left(\frac{\Delta PC}{P}\right)_{ik}\theta_{ik}^{-}}{\sum_{k=1}^{Q}\theta_{ik}^{-}} \quad \text{(Eq. 17)}$$

Multiple-per-rev = MPR = 1 for this case.

4.1.2.2 Patterns with $\theta_{ik}^{+} > \theta_{min}^{+}$

If the pattern has low-pressure regions circumferentially separated by high-pressure regions with extents greater than θ_{min}^{+} then the multiple-per-revolution element is greater than one.

Intensity $\left(\frac{\Delta PC}{P}\right)_i$ is the $\left(\frac{\Delta PC}{P}\right)_{ik}$ corresponding to the maximum value of $\left[\left(\frac{\Delta PC}{P}\right)_{ik}\theta_{ik}^{-}\right]$.

Extent θ_i^{-} is the θ_{ik}^{-} corresponding to the maximum value of $\left[\left(\frac{\Delta PC}{P}\right)_{ik}\theta_{ik}^{-}\right]$.

The multiple-per-revolution term is defined as the number of equivalent low-pressure regions, the equivalence being based on the ratio of the total integrated area beneath $(PAV)_i$ in Figure 5 to the largest single area beneath $(PAV)_i$. This is given by the equation:

$$\text{Multiple - per - revolution} = (MPR)_i = \frac{\sum_{k=1}^{Q}\left[\left(\frac{\Delta PC}{P}\right)_{ik}\theta_{ik}^{-}\right]}{\max\left[\left(\frac{\Delta PC}{P}\right)_{ik}\theta_{ik}^{-}\right]} \quad \text{(Eq. 18)}$$

4.1.3 Radial Distortion Elements

The radial distortion intensity of a ring is defined as the difference between the face-average pressure and the ring-average pressure divided by the face-average pressure. Both positive and negative values of radial intensity therefore occur; positive values reflect a ring-average pressure that is below the face average. A typical tip-radial distortion pattern is shown in Figure 6. The arrows indicate the difference in radial pressure for ring 5. For the general ring, i, the radial intensity is given as:

$$\left(\frac{\Delta PR}{P}\right)_i = \frac{(PFAV) - (PAV)_i}{(PFAV)} \quad \text{(Eq. 19)}$$

where:

PFAV is the area-weighted face-average pressure. For N rings at centers of equal areas:

$$PFAV = \frac{1}{N}\sum_{i=1}^{N}(PAV)_i \quad \text{(Eq. 20)}$$

It should be noted that the definition of the radial intensity implies that $\frac{1}{N}\sum_{i=1}^{N}\left(\frac{\Delta PR}{P}\right)_i = 0$.

AVA Documents Document Sharing Hub

Full document details: SAE AIR1419D

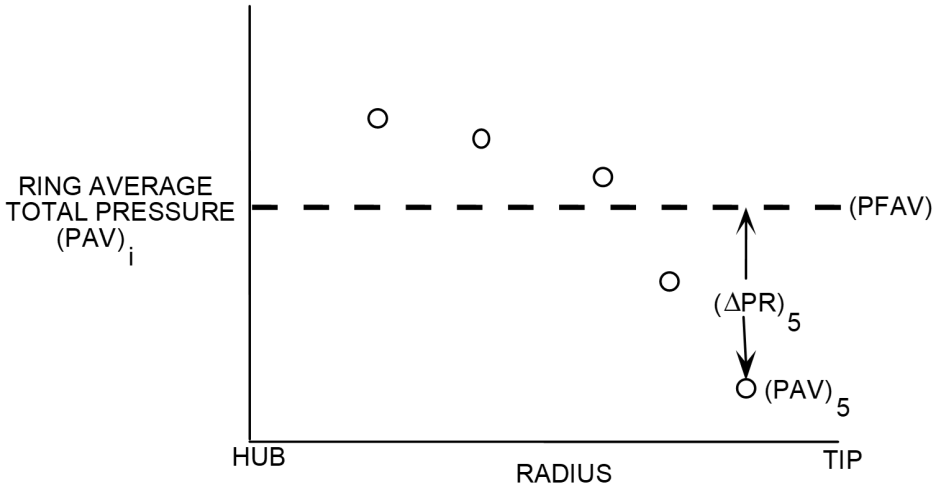


Figure 6 - Radial distortion pattern

4.2 Rationale for Element Definitions

The definitions of the distortion-descriptor elements given in 4.1 were chosen for a number of reasons. The most important requirement was that the elements should describe well-established facts, that is, the stability of an engine compression component is sensitive to the magnitude of a circumferentially varying total-pressure defect (circumferential intensity), the time a blade spends in the defect region (extent), the number of defects encountered by a blade in one revolution (multiple-per-rev), the magnitude of a radially-varying total-pressure defect (radial intensity), and whether the circumferential and/or radial defects occur in the hub, mid-span, or tip regions of the compression-component inlet (refer to SAE 680286).

The particular form of the circumferential distortion intensity element was chosen to aid in making hand calculations by avoiding complicated mathematical expansions and to avoid sensitivity to a single-probe low total-pressure reading. The latter was accomplished by averaging the pressures in the low total-pressure region, thus avoiding an expression such as $(P_{MAX} - P_{MIN})/P_{AVG}$ which is descriptive of the flow, but does not take the response of the turbomachinery into account. The circumferential intensity element was nondimensionalized by the ring-average total pressure rather than face-average total pressure in an attempt to reduce the apparent “double bookkeeping” that occurs when analyzing complex aircraft patterns. This “double bookkeeping” occurs when the low total-pressure region may contribute to both the circumferential and radial intensity elements so as to effectively make the defect appear more severe than it actually is.

To reduce the computation time for the time-variant distortion descriptor elements, linear interpolation is considered adequate for determining the angular extent (θ^-) of a low-pressure region, thus avoiding differing results due to the type of interpolation used (Fourier curve fit, polynomial, spline). This pragmatic approach to handling large amounts of data produces results that correlate to an acceptable degree of accuracy.

A continuous functional representation, indicating the presence of multiple-per-rev regions, rather than an integer jump function, was chosen because the stability response of compression components varies in a continuous manner, depending on the relationship between the intensity-extent products for each of the low-pressure regions.

4.3 Sample Element Calculations

As an aid to interpreting and calculating the distortion-descriptor elements, an example inlet pattern, illustrated in Figure 7, is examined in detail. The corresponding probe readings, normalized by face-average total pressure, are given in Figure 8. The pattern has two low pressure regions separated by more than 25 degrees in the outer rings and is termed a “two-per-rev pattern.” The ARP1420 recommended probe array is superposed. The calculation of the circumferential distortion elements for the inner ring where the circumferential profile is only a one-per-rev profile is illustrated in Figure 9. The intensity element (ΔPC/P) is 0.02 per Equations 10 and 12. The extent element (θ^-) is 157 degrees and the multiple-per-rev element (MPR) is 1.0 per Equation 13. The calculation of the circumferential distortion elements for the outer ring is illustrated in Figure 10. This ring has two low-pressure regions separated by more than θ^+_{min}. In this case, the intensity is equal to the value associated with the largest area under the ring-average total pressure. The multiple-per-rev factor is equal to 1.1 per Equation 18. The values of the radial distortion elements, as calculated according to Equation 19, are illustrated in Figure 11.

AVA Documents Document Sharing Hub

Full document details: SAE AIR1419D

All distortion elements for each ring of this pattern can be illustrated using a bar graph display as shown in Figure 12. This type of display makes it possible to obtain quickly the following characteristics of the pattern:

a. The circumferential intensity is greatest at the tip.

b. The circumferential extent is greatest at the hub.

c. The only multiple-per-rev content exists at the tip.

d. The radial intensity is greatest at the tip.

This format gives the data and the results in both tabular and pictorial form and will be used to summarize the data and the results for the sample distortion patterns of the next subsection. The data for this example as well as the results are given in Figure 8.

A pattern with two low-pressure regions separated by less than θ_{min}^{+} is illustrated in Figure 13. The circumferential distortion intensity element for the outer ring was calculated according to Equation 15 and has a value of 0.026.

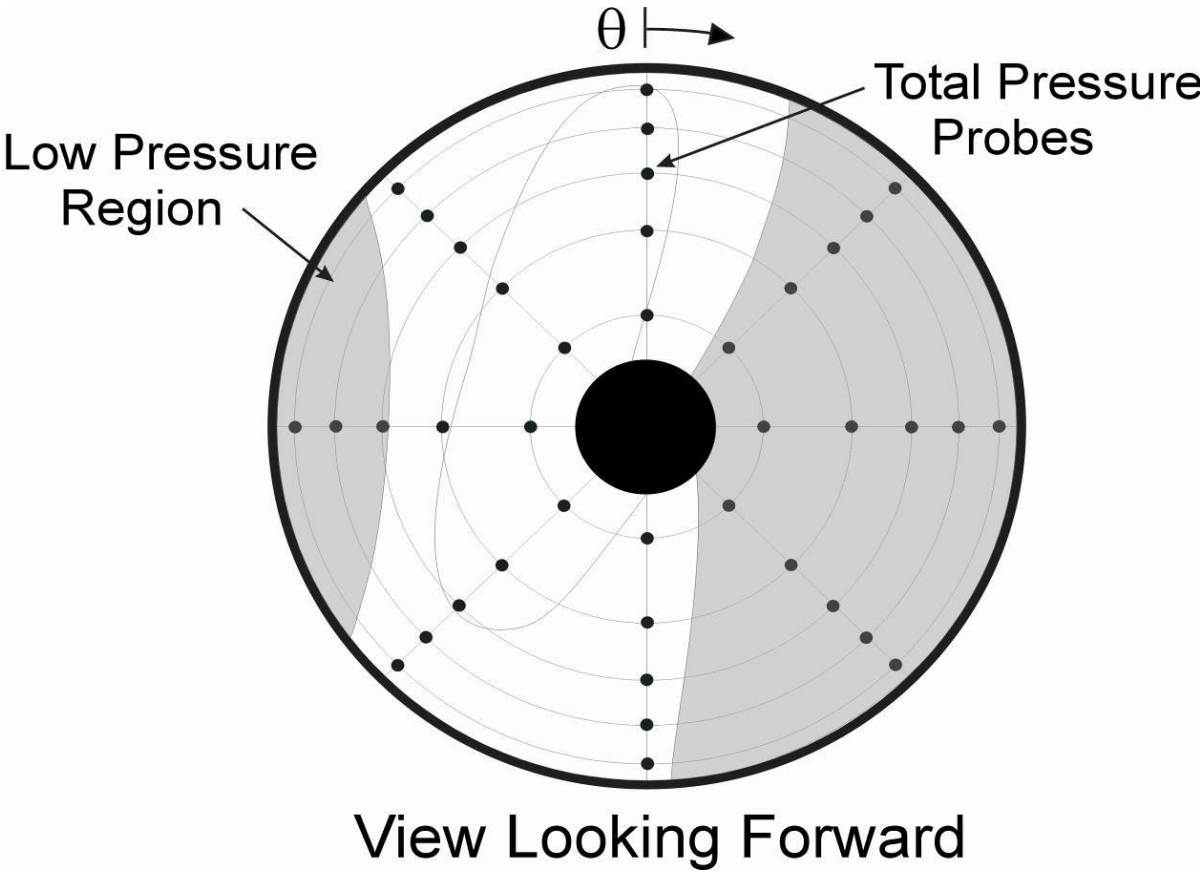
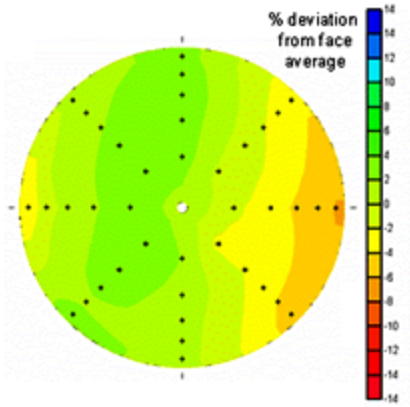


Figure 7 - Example of inlet pattern

Documents
Document Sharing Hub
Full document details: SAE AIR1419D

Probe by Probe
Clockwise from TDC

	rake 1	rake 2	rake 3	rake 4	rake 5	rake 6	rake 7	rake 8
ring 1 (hub)	1.021	0.987	0.976	0.985	1.010	1.028	1.024	1.028
ring 2	1.024	0.980	0.960	0.970	1.005	1.020	1.008	1.018
ring 3	1.027	0.972	0.948	0.960	1.001	1.017	0.995	1.010
ring 4	1.025	0.963	0.938	0.950	1.000	1.006	0.985	1.004
ring 5 (tip)	1.020	0.957	0.930	0.942	1.000	1.024	0.952	0.998



Distortion Descriptor Elements

	$\left(\frac{\Delta PC}{P}\right)_i$	$(\theta^*)_i$	$(MPR)_i$	$\left(\frac{\Delta PR}{P}\right)_i$
ring 1	0.0196	157.2	1.0000	-0.0158
ring 2	0.0238	144.7	1.0000	-0.0065
ring 3	0.0272	140.0	1.0000	0.0005
ring 4	0.0298	135.6	1.0000	0.0079
ring 5	0.0315	132.7	1.1313	0.0139

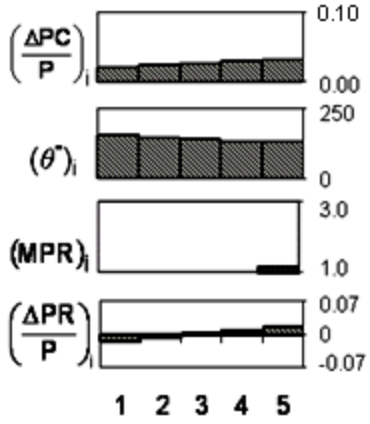


Figure 8 - Sample pattern definition and results

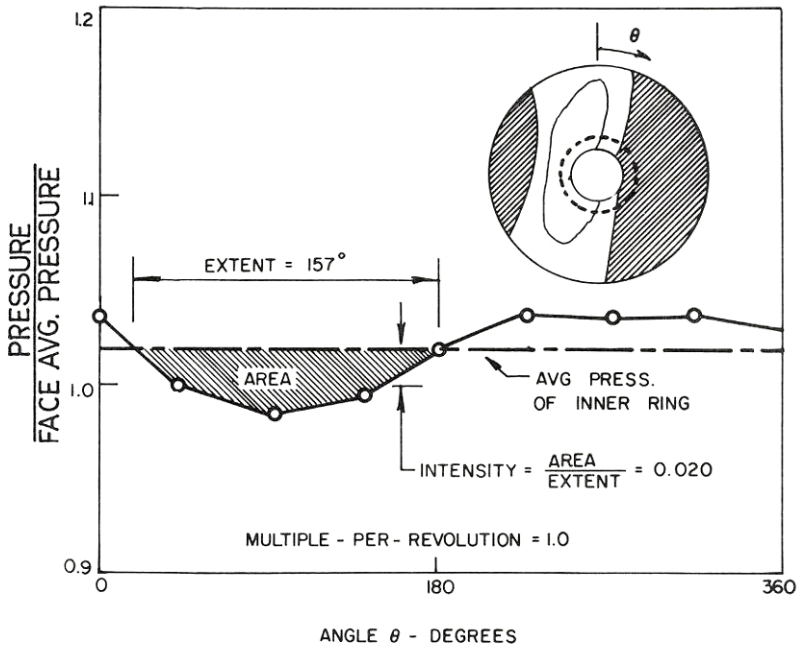


Figure 9 - Circumferential distortion elements for inner ring

Documents
Document Sharing Hub
Full document details: SAE AIR1419D

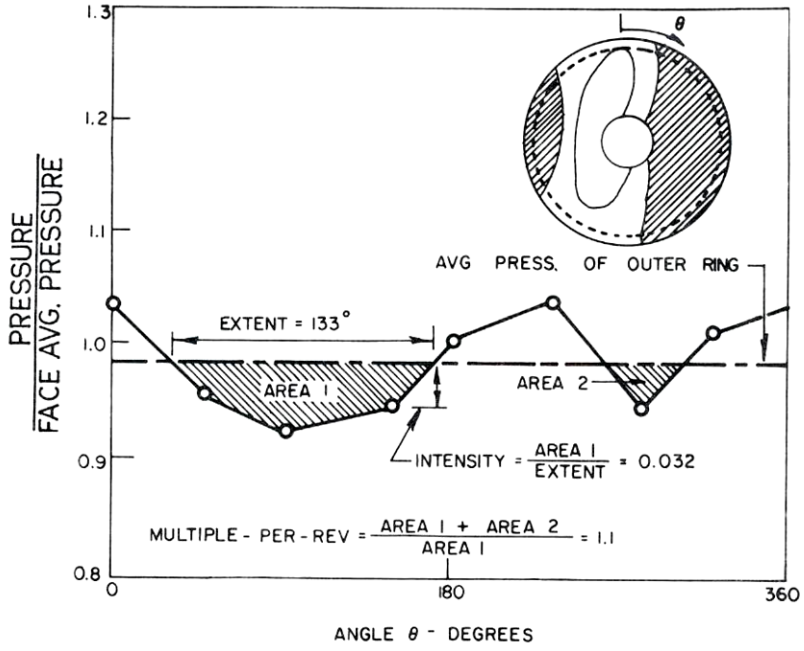


Figure 10 - Circumferential distortion elements for outer ring

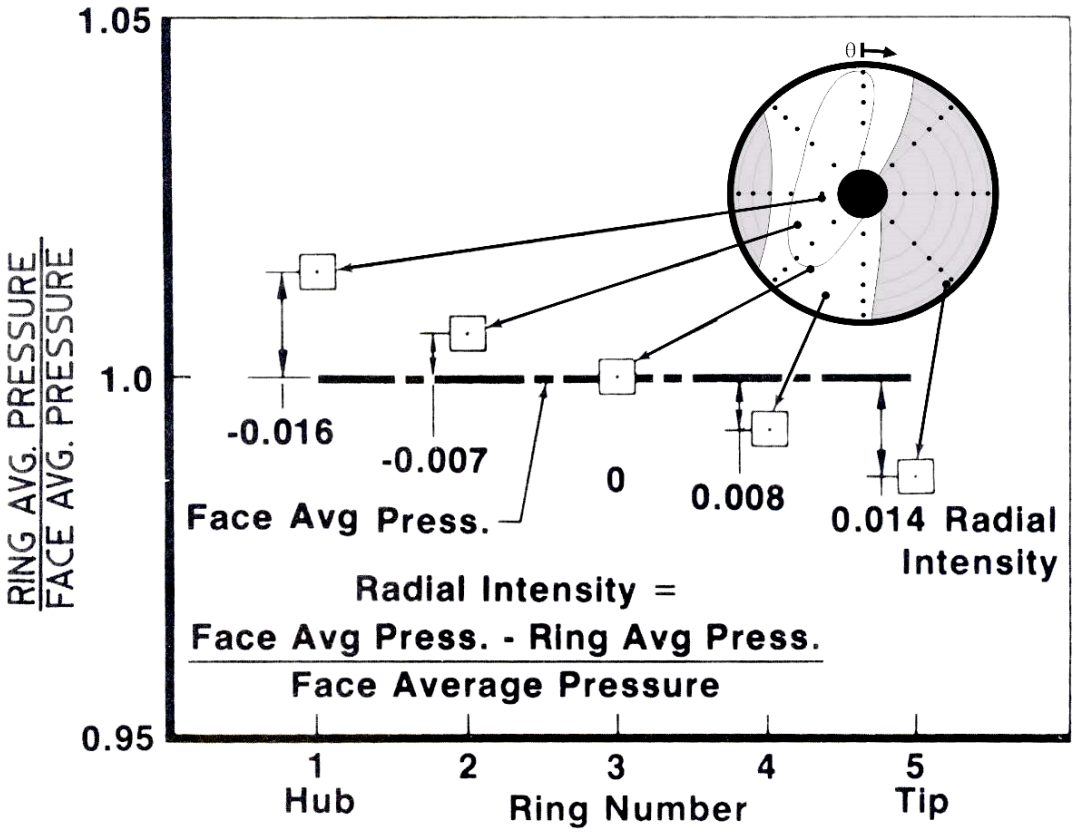


Figure 11 - Radial distortion elements

Documents
Document Sharing Hub
Full document details: SAE AIR1419D

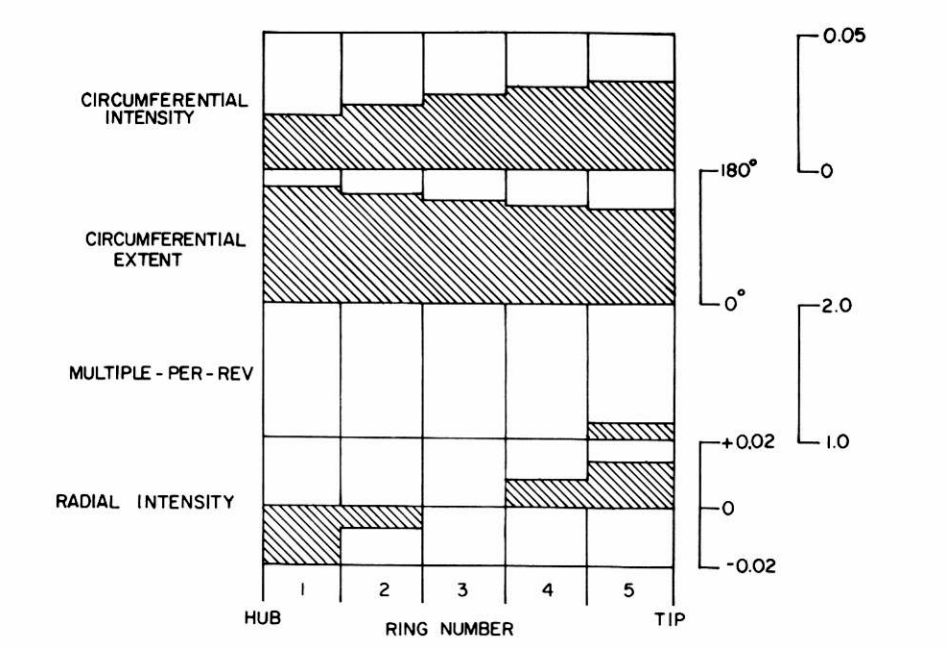


Figure 12 - Distortion-descriptor elements for the example inlet pattern

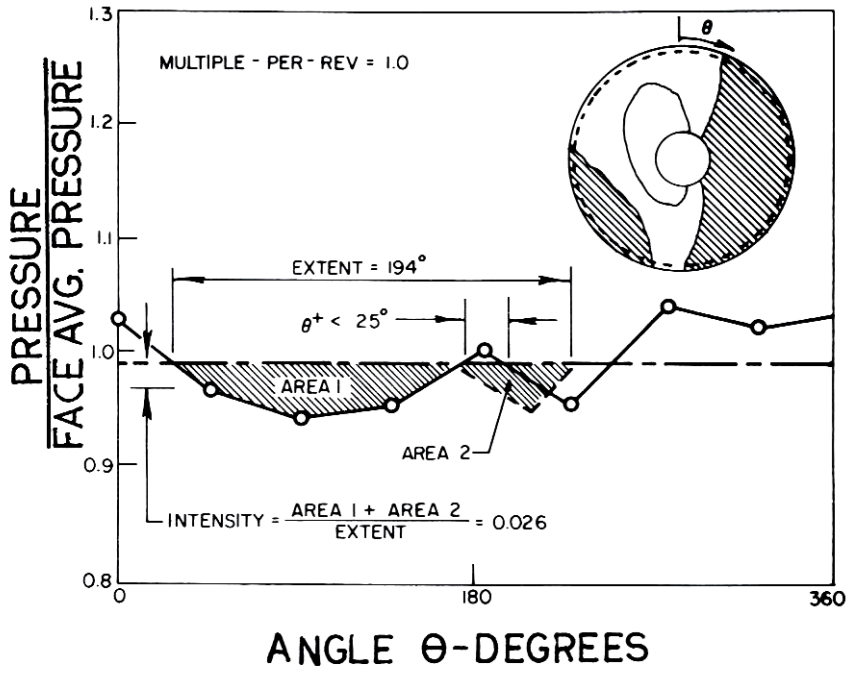


Figure 13 - Equivalent one-per-rev pattern

Documents
Document Sharing Hub
Full document details: SAE AIR1419D

4.4 Example Distortion Patterns

Example distortion patterns are given in this paragraph for use in checking computer program results and to illustrate the results obtained when calculating the distortion descriptor elements for each of the patterns. The elements of the probe-by-probe data arrays are the probe readings normalized by the area-weighted face-average total pressure.

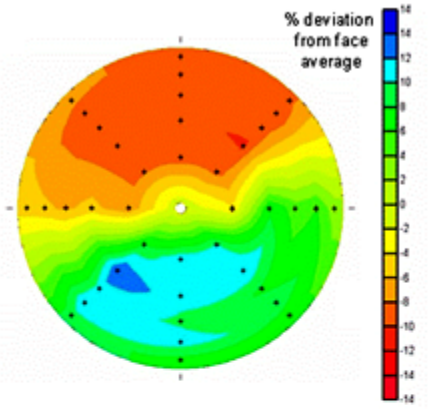
Each of these patterns is taken from screen test data. Although the patterns of 4.4.1 through 4.4.6 were intended to be classical patterns (180 degrees one-per-rev square wave, hub-radial, and tip-radial), and/or stylized combined patterns (180 degrees one-per-rev + hub-radial, 180 degrees one-per-rev + tip-radial, and 90 degrees one-per-rev + tip-radial), the actual patterns often had significant differences from the intended patterns. Careful attention to detail is required when designing a distortion screen if the desired pattern shapes and distortion element values are to be achieved for all test conditions.

4.4.1 180 Degrees One-Per-Rev Circumferential Distortion Pattern

The information relevant to this pattern is given in Figure 14. The ring circumferential intensity values are nearly constant and the angular extent of the circumferential distortion is uniform from ring-to-ring. There is no multiple-per-rev content and very little radial distortion content.

Probe by Probe
Clockwise from TDC

	rake 1	rake 2	rake 3	rake 4	rake 5	rake 6	rake 7	rake 8
ring 1 (hub)	0.906	0.912	0.962	1.101	1.116	1.079	0.924	0.915
ring 2	0.903	0.897	1.075	1.119	1.103	1.139	0.946	0.902
ring 3	0.905	0.904	1.048	1.076	1.096	1.107	0.935	0.907
ring 4	0.906	0.899	1.058	1.090	1.107	1.115	0.943	0.905
ring 5 (tip)	0.908	0.914	1.028	1.069	1.071	1.090	0.949	0.925



Distortion Descriptor Elements

	$\left(\frac{\Delta PC}{P}\right)_i$	$(\theta^*)_i$	$(MPR)_i$	$\left(\frac{\Delta PR}{P}\right)_i$
ring 1	0.0652	207.8	1.0000	0.0095
ring 2	0.0877	178.7	1.0000	-0.0117
ring 3	0.0755	180.4	1.0000	0.0016
ring 4	0.0800	180.1	1.0000	-0.0040
ring 5	0.0634	181.1	1.0000	0.0046

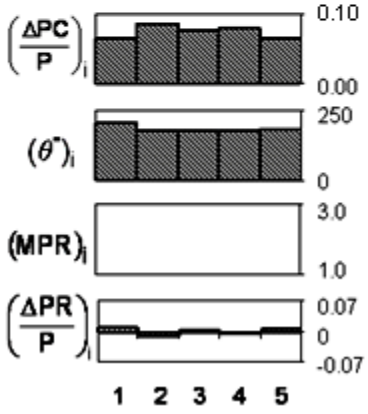


Figure 14 - 180 degrees 1/rev circumferential distortion pattern

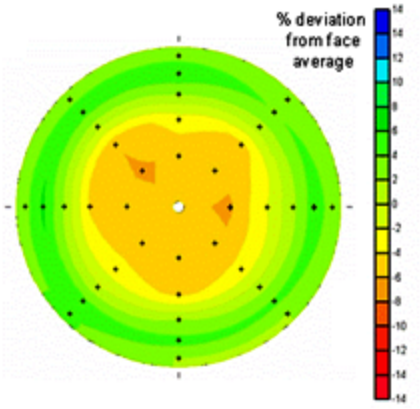
Documents
Document Sharing Hub
Full document details: SAE AIR1419D

4.4.2 Hub-Radial Distortion Pattern

The information relevant to this pattern is given in Figure 15. This hub-radial pattern has almost no circumferential distortion. The angular extent and multiple-per-rev elements have little physical significance.

Probe by Probe
Clockwise from TDC

	rake 1	rake 2	rake 3	rake 4	rake 5	rake 6	rake 7	rake 8
ring 1 (hub)	0.943	0.944	0.938	0.942	0.945	0.946	0.947	0.938
ring 2	0.972	0.955	0.982	0.967	0.957	0.968	0.959	0.941
ring 3	1.023	1.013	1.017	1.011	1.021	1.003	1.020	1.007
ring 4	1.058	1.038	1.053	1.045	1.048	1.050	1.063	1.051
ring 5 (tip)	1.031	1.026	1.030	1.020	1.019	1.043	1.032	1.035



Distortion Descriptor Elements

	$\left(\frac{\Delta PC}{P}\right)_i$	$(\theta^{\sim})_i$	$(MPR)_i$	$\left(\frac{\Delta PR}{P}\right)_i$
ring 1	0.0025	94.7	1.7419	0.0571
ring 2	0.0103	94.5	1.2779	0.0374
ring 3	0.0056	58.5	1.7627	-0.0143
ring 4	0.0039	191.9	1.0000	-0.0507
ring 5	0.0048	178.3	1.0000	-0.0295

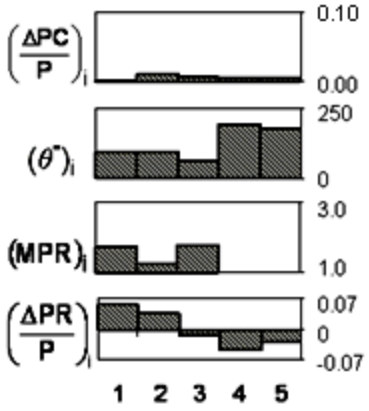


Figure 15 - Hub-radial distortion pattern

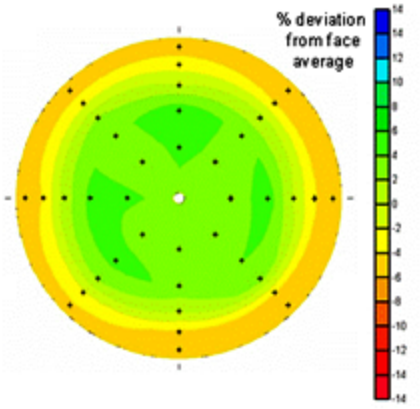
Documents
Document Sharing Hub
Full document details: SAE AIR1419D

4.4.3 Tip-Radial Distortion Pattern

The information relevant to this pattern is given in Figure 16. This tip-radial pattern has essentially no circumferential distortion. The angular extent and multiple-per-rev elements have little physical significance.

Probe by Probe
Clockwise from TDC

	rake 1	rake 2	rake 3	rake 4	rake 5	rake 6	rake 7	rake 8
ring 1 (hub)	1.044	1.037	1.028	1.030	1.038	1.032	1.043	1.032
ring 2	1.054	1.033	1.051	1.040	1.035	1.048	1.045	1.034
ring 3	1.000	1.010	0.997	1.029	1.002	1.022	1.008	1.021
ring 4	0.970	0.960	0.961	0.960	0.954	0.976	0.960	0.975
ring 5 (tip)	0.948	0.943	0.943	0.943	0.945	0.954	0.952	0.945



Distortion Descriptor Elements

	$\left(\frac{\Delta PC}{P}\right)_i$	$(\theta^{\sim})_i$	$(MPR)_i$	$\left(\frac{\Delta PR}{P}\right)_i$
ring 1	0.0044	113.4	1.2297	-0.0354
ring 2	0.0040	81.2	2.3086	-0.0424
ring 3	0.0066	133.7	1.2195	-0.0111
ring 4	0.0050	176.7	1.0687	0.0356
ring 5	0.0031	175.7	1.0555	0.0534

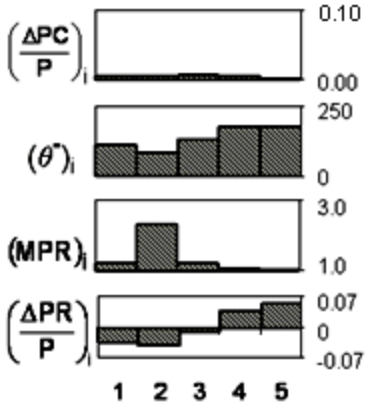


Figure 16 - Tip-radial distortion pattern

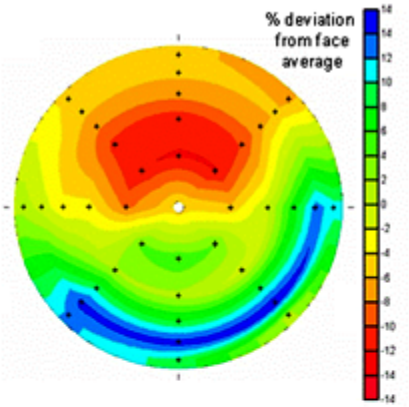
Documents
Document Sharing Hub
Full document details: SAE AIR1419D

4.4.4 180 Degrees One-Per-Rev + Hub-Radial Combined Distortion Pattern

The information relevant to this pattern is given in Figure 17. This 180 degrees one-per-rev + hub-radial combined distortion pattern has fairly uniform circumferential angular extent, and tip-radial distortion intensity elements. There is minor multiple-per-rev content in the tip.

Probe by Probe
Clockwise from TDC

	rake 1	rake 2	rake 3	rake 4	rake 5	rake 6	rake 7	rake 8
ring 1 (hub)	0.874	0.874	0.941	1.035	1.050	1.037	0.910	0.877
ring 2	0.884	0.898	0.996	0.988	1.009	1.013	0.965	0.889
ring 3	0.925	0.930	1.067	1.086	1.077	1.090	0.961	0.920
ring 4	0.940	0.938	1.124	1.151	1.143	1.140	0.986	0.942
ring 5 (tip)	0.938	0.930	1.104	1.010	1.086	1.120	1.007	0.949



Distortion Descriptor Elements

	$\left(\frac{\Delta PC}{P}\right)_i$	$(\theta^-)_i$	$(MPR)_i$	$\left(\frac{\Delta PR}{P}\right)_i$
ring 1	0.0610	198.3	1.0000	0.0456
ring 2	0.0541	155.5	1.0000	0.0400
ring 3	0.0660	176.3	1.0000	-0.0120
ring 4	0.0808	178.4	1.0000	-0.0506
ring 5	0.0603	162.1	1.0034	-0.0230

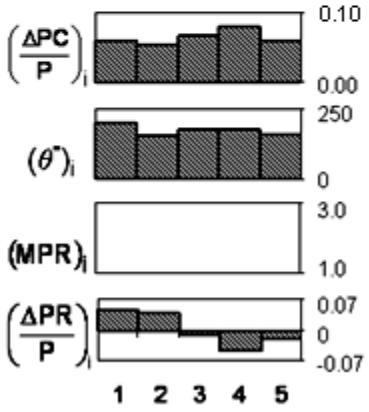


Figure 17 - 180 degrees 1/rev + hub-radial combined distortion pattern

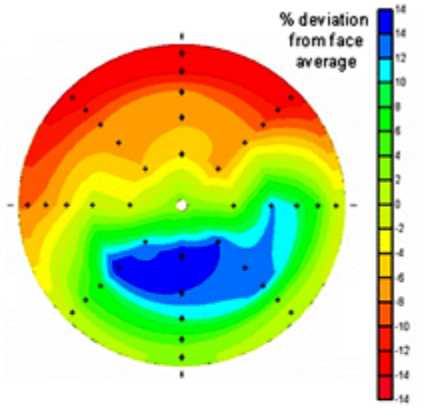
Documents
Document Sharing Hub
Full document details: SAE AIR1419D

4.4.5 180 Degrees One-Per-Rev + Tip-Radial Combined Distortion Pattern

The information relevant to this pattern is given in Figure 18. This 180 degrees one-per-rev + tip-radial combined distortion pattern has fairly uniform circumferential and angular extent distortion elements. There is no multiple-per-rev content. The tip-radial-distortion content is not as uniform as might be desired.

Probe by Probe
Clockwise from TDC

	rake 1	rake 2	rake 3	rake 4	rake 5	rake 6	rake 7	rake 8
ring 1 (hub)	0.961	0.936	1.024	1.144	1.175	1.120	0.988	0.947
ring 2	0.939	0.943	1.128	1.131	1.143	1.166	1.000	0.930
ring 3	0.927	0.910	1.102	1.131	1.104	1.082	0.958	0.924
ring 4	0.876	0.885	1.062	1.041	1.050	1.057	0.931	0.889
ring 5 (tip)	0.873	0.871	1.002	1.006	1.032	1.006	0.921	0.868



Distortion Descriptor Elements

	$\left(\frac{\Delta PC}{P}\right)_i$	$(\theta^-)_i$	$(MPR)_i$	$\left(\frac{\Delta PR}{P}\right)_i$
ring 1	0.0662	201.5	1.0000	-0.0322
ring 2	0.0839	173.3	1.0000	-0.0427
ring 3	0.0757	181.6	1.0000	-0.0126
ring 4	0.0744	172.9	1.0000	0.0306
ring 5	0.0628	175.2	1.0000	0.0569

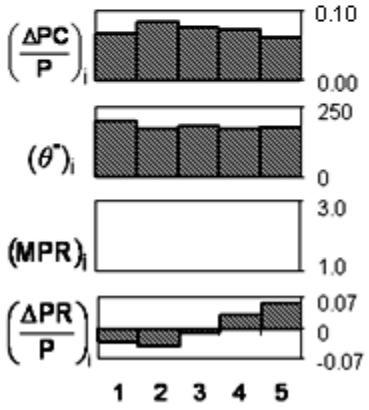


Figure 18 - 180 degrees 1/rev + tip-radial combined distortion pattern

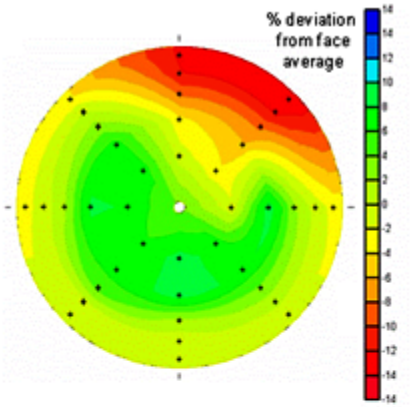
Documents
Document Sharing Hub
Full document details: SAE AIR1419D

4.4.6 90 Degrees One-Per-Rev + Tip-Radial Combined Distortion Pattern

The information relevant to this pattern is given in Figure 19. This 90 degrees one-per-rev + tip-radial combined distortion pattern has essentially uniform circumferential and angular extent distortion elements. There is no multiple-per-rev content in this pattern. The nonuniformity of the tip-radial content is similar to that of the 180 degrees one-per-rev + tip-radial combined distortion pattern.

Probe by Probe
Clockwise from TDC

	rake 1	rake 2	rake 3	rake 4	rake 5	rake 6	rake 7	rake 8
ring 1 (hub)	0.987	0.962	0.982	1.068	1.086	1.061	1.076	1.069
ring 2	0.961	0.939	1.091	1.072	1.086	1.064	1.080	1.064
ring 3	0.911	0.913	1.020	1.034	1.010	1.046	1.012	1.026
ring 4	0.878	0.873	0.989	1.002	0.984	0.987	0.985	0.997
ring 5 (tip)	0.872	0.858	0.970	0.983	0.981	0.985	0.972	0.961



Distortion Descriptor Elements

	$\left(\frac{\Delta PC}{P}\right)_i$	$(\theta^*)_i$	$(MPR)_i$	$\left(\frac{\Delta PR}{P}\right)_i$
ring 1	0.0472	145.5	1.0000	-0.0390
ring 2	0.0631	112.8	1.0000	-0.0473
ring 3	0.0592	113.6	1.0000	0.0009
ring 4	0.0631	111.2	1.0000	0.0356
ring 5	0.0600	119.4	1.0000	0.0498

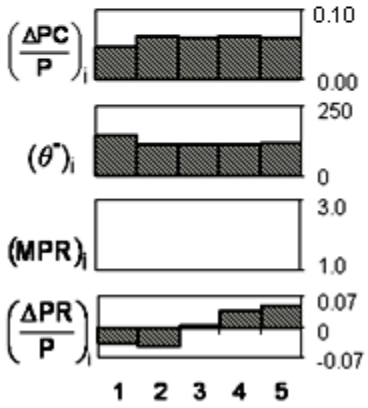


Figure 19 - 90 degrees 1/rev + tip-radial combined distortion pattern

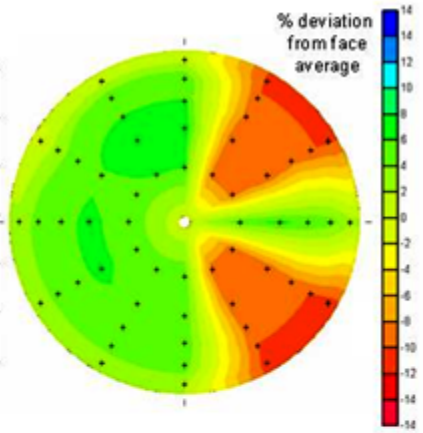
Documents
Document Sharing Hub
Full document details: SAE AIR1419D

4.4.7 Two-Per-Rev with Lows Closer than 25 Degrees and with Tip-Radial Distortion Pattern

The information relevant to this pattern is given in Figure 20. This pattern is treated as a one-per-rev pattern which has a nearly uniform circumferential extent of approximately 140 degrees. The circumferential distortion level is nearly uniform ring-to-ring with a value of approximately 0.07, and the radial distortion is located at the tip with a value of approximately 0.02.

Probe by Probe
Clockwise from TDC

	rake 1	rake 2	rake 3	rake 4	rake 5	rake 6	rake 7	rake 8	rake 9	rake 10	rake 11	rake 12
ring 1 (hub)	1.060	0.911	0.911	1.056	0.905	0.905	1.055	1.055	1.056	1.056	1.057	1.060
ring 2	1.073	0.900	0.900	1.062	0.903	0.903	1.056	1.056	1.062	1.062	1.058	1.073
ring 3	1.060	0.911	0.911	1.057	0.907	0.907	1.059	1.059	1.057	1.057	1.056	1.060
ring 4	1.058	0.902	0.902	1.049	0.899	0.899	1.052	1.052	1.049	1.049	1.029	1.058
ring 5 (tip)	1.010	0.895	0.895	1.026	0.889	0.889	1.021	1.021	1.026	1.026	0.998	1.010



Distortion Descriptor Elements

	$\left(\frac{\Delta PC}{P}\right)_i$	$(\theta^-)_i$	$(MPR)_i$	$\left(\frac{\Delta PR}{P}\right)_i$
ring 1	0.0704	140.1	1.0000	-0.0072
ring 2	0.0761	139.9	1.0000	-0.0090
ring 3	0.0704	139.9	1.0000	-0.0084
ring 4	0.0712	138.7	1.0000	0.0002
ring 5	0.0614	138.0	1.0000	0.0245

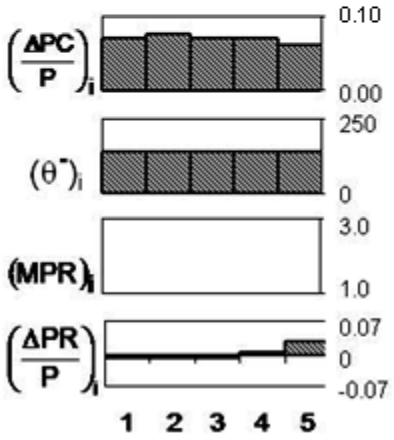


Figure 20 - Two/rev with lows closer than 25 degrees and with tip-radial distortion pattern

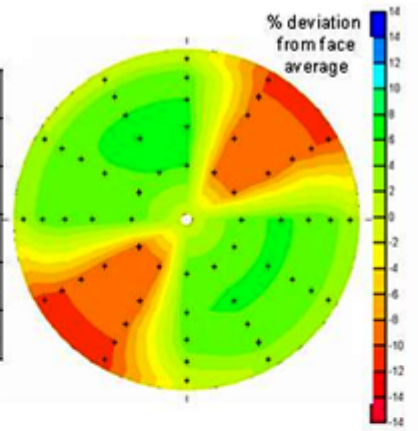
Documents
Document Sharing Hub
Full document details: SAE AIR1419D

4.4.8 Two-Per-Rev with Lows Further Apart than 25 Degrees and with Tip-Radial Distortion Pattern

The information relative to this pattern is given in Figure 21. The multiple-per-rev descriptor element for this pattern has a value of almost two, making it a “bona fide” two-per-rev pattern. The extent of the largest low-pressure region is approximately 71 degrees. The circumferential distortion is essentially uniform from hub to tip with a value of approximately 0.07 and a tip-radial-distortion value of approximately 0.02.

Probe by Probe
Clockwise from TDC

	rake 1	rake 2	rake 3	rake 4	rake 5	rake 6	rake 7	rake 8	rake 9	rake 10	rake 11	rake 12
ring 1 (hub)	1.060	0.911	0.911	1.056	1.056	1.056	1.057	0.905	0.905	1.055	1.055	1.060
ring 2	1.073	0.900	0.900	1.062	1.062	1.062	1.058	0.903	0.903	1.056	1.056	1.073
ring 3	1.060	0.911	0.911	1.057	1.057	1.057	1.054	0.907	0.907	1.059	1.059	1.060
ring 4	1.058	0.902	0.902	1.049	1.049	1.049	1.029	0.899	0.899	1.052	1.052	1.058
ring 5 (tip)	1.010	0.895	0.895	1.026	1.026	1.026	0.998	0.889	0.889	1.021	1.021	1.010



Distortion Descriptor Elements

	$\left(\frac{\Delta PC}{P}\right)_i$	$(\bar{\theta})_i$	$(MPR)_i$	$\left(\frac{\Delta PR}{P}\right)_i$
ring 1	0.0723	70.6	1.9288	-0.0073
ring 2	0.0775	69.1	1.9942	-0.0090
ring 3	0.0715	70.6	1.9502	-0.0083
ring 4	0.0711	73.0	1.9301	0.0001
ring 5	0.0624	73.5	1.8944	0.0245

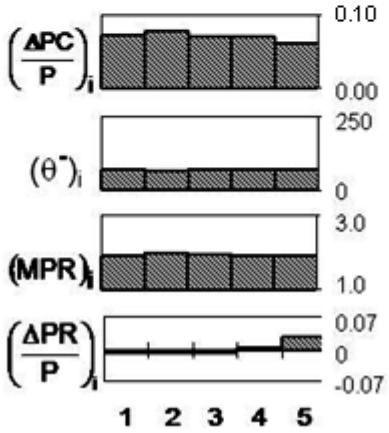


Figure 21 - Two/rev with lows further apart than 25 degrees and with tip-radial distortion pattern

Documents
Document Sharing Hub
Full document details: SAE AIR1419D